Author Response to Reviewer 2

Responses are shown in **blue**, and excerpts from the revised manuscript are shown in **red**.

> The manuscript entitles "Ultra-Lightweight Mid-IR Methane Sensor for UAV-based Measurements" by Beattie et al. presents an absorption spectrometer designed for airborne in-situ measurements on a small UAV platform. The study describes the optical and technical design of the sensor for methane detection and evaluates its instrumental performance through laboratory and field experiments. In addition, two field missions are presented in which methane plumes from controlled-release point sources are measured, and corresponding fluxes are derived using a curtain flux approach.
>
> This manuscript is well written and presents an integrated work of instrument development and characterization to first field missions; however, it lacks of detailed method descriptions, instrument uncertainty characterizations, and analytical tests.
>
> After major revision, this manuscript might be suitable for publication.

We thank the reviewer for their detailed and thoughtful comments. We greatly appreciate their insights and their time in reviewing our work. We have incorporated the Reviewer's feedback, including additional method descriptions, uncertainty characterizations, and analytical test results, and we feel that the revised manuscript is much improved as a result.

> **General comments:**
>
> The authors use throughout the whole manuscript the wording "concentrations", even though the data is shown in mixing ratios (ppm or ppb). Mixing ratios are converted into concentration for the flux estimation, as also described in Section 2.7; however, the detection is via mixing ratios. The authors should not confuse this and stick to mixing ratios, when they report the values in ppm or ppb.

We thank the reviewer for their attention to the terminology. Throughout the manuscript, the term "concentration" has been replaced with "mole fraction."

> The manuscript would benefit from including more literature, especially in the introduction and the discussions. This sensor is not the first small and lightweight airborne absorption spectrometer (e.g., D'Amato et al., 2025). The authors should consider to compare their sensor to similar instrumentation, highlighting the specific advantages and limitations of the presented instrument relative to existing systems.

We have expanded on the discussion of similar instrumentation in the introduction, focusing on lightweight spectrometers that have been deployed on UAVs. The revised text is below:

L. 80-107: "Several methane sensing instruments based on tunable diode laser absorption spectroscopy (TDLAS) have been developed for UAVs. Nathan et al. (2015) developed an open-path sensor employing a near-infrared (1651 nm) diode laser light source in wavelength modulation spectroscopy (WMS) mode and deployed it on an electric fixed-wing model aircraft with a wing span of 3 m. The sensor weighed 3.1 kg with a 1 Hz precision of 100 ppb and a power consumption of 25 W. Golston et al. (2017) used a mid-IR diode laser (3270 nm) in WMS mode for their open-path instruments. Two versions of the sensor were reported for fixed-wing and rotary-wing UAVs weighing 4.7 kg and 1.6 kg, inclusive of batteries, with reported precisions of 5 ppb and 10 ppb at 1 Hz, respectively. The sensor power consumption was reported to be 30 W. Bonne et al. (2024) also used mid-IR open-path TDLAS for their combined CH_4 and CO_2 sensor. The sensor employed direct absorption spectroscopy (DAS), weighed 1.4 kg (not including dedicated batteries), had a 1 Hz precision of 10 ppb for CH_4 detection, and consumed 8 to 15 W of power. Smith et al. (2023) report open- and closed-path TDLAS instruments that were developed for fixed-wing and rotary-wing UAVs. The sensors weigh 0.6 and 0.85 kg with reported 1 Hz precisions of 40 ppb and 164 ppb, respectively. Shah et al. (2020) developed a closed-path near-IR TDLAS instrument that employs the off-axis integrated cavity output spectroscopy (ICOS) sensing technique. The sensor weighs 3.4 kg, has a 1 Hz precision of 2.2 ppb, and a power consumption of 32 W. Commercially available MIRA Pico and MIRA Strato mid-IR sensors from Aeris Technologies (USA) have also been deployed on UAVs (Dooley et al., 2024; Bolek et al., 2024, 2026). These sensors employ DAS, weigh 3 kg and 2 kg, respectively, and have reported 1 Hz precisions of <1 ppb and <2 ppb. Their steady state power consumption is in the range of 15-18 W.

Gas sensors based on quantum cascade laser absorption spectroscopy (QCLAS) have also been developed for aerial platforms (D'Amato et al. 2025; Tuzson et al. (2020). Quantum cascade lasers (QCLs) extend further into the mid-infrared wavelength range than tunable diode lasers (TDLs), which is advantageous for gas spectroscopy, where many gases exhibit the strongest absorbance in the mid-infrared (3 to 20 μm) (D'Amato et al., 2025). For methane, however, the strongest absorbance is found in the ν_3

fundamental C-H stretching mode near 3.3 µm (Dang-Nhu et al., 1979), which is accessible to both QCLs and TDLs. QCLs are typically more expensive than TDLs and have much higher power consumption when operating in continuous-wave mode (D'Amato et al., 2025). As such, TDLs are a more popular choice for methane gas spectroscopy than QCLs. One notable lightweight QCLAS methane sensor that was designed for UAV applications was developed by Tuzson et al. (2020). This instrument targeted methane's mid-infrared absorption line at 7.83 µm. The sensor weighed 2.1 kg (including the battery) and had a reported 1 Hz precision of 1.1 ppb. Its power consumption was 18 W, enabled using an intermittent continuous-wave laser driving approach."

We also compare back to these instruments in the Methods and Results sections. Relevant text is below:

L. 221-224: "As one of the lightest methane gas spectrometers developed to date, the instrument is well within the payload limits of many small consumer- or enterprise-grade UAVs such as the DJI Matrice 300 RTK used in this study, allowing for simultaneous deployment of an on-board anemometer system on a highly portable measurement platform, as described in Section 2.5."

L. 357-360: "The 1 s averaging times (in-flight precision: 6.6 ppb; laboratory precision: 3.7 ppb) represent a useful metric for comparison to other lightweight UAV sensors. Though other instruments offer slightly smaller 1 s precisions in the range of 1-5 ppb, to our knowledge the ultra-lightweight sensor presented here offers the best 1 s precision for a sub-2 kg methane sensor reported to date."

L. 504-507: "Drift is known to affect other UAV-borne sensors including commercial instruments such as the Aeris MIRA Pico and Strato sensors (Dooley et al., 2024; Bolek et al., 2026). Notably, Dooley et al., (2024) showed a systematic drift of roughly 250 ppb over a 20-minute UAV flight for a MIRA Pico sensor."

> The authors should include more discussion on the instrument's performance regarding uncertainty contributions. Literature has shown that laboratory performance cannot be assumed for field operation, particularly for airborne platforms (Werle et al., 1993, 2011, Röder et al., 2024, Ort et al., 2024). The authors already included the Allen-Werle plot for both, laboratory and field operation; however, optimum integration times and precisions are stated, but not discussed regarding their error contributions. Please state somewhere, what you mean with "ambient methane values" and how you defined those during both timeseries used for the Allan deviation. Were laboratory tests made to quantify the effects of pressure, temperature, and water vapor on the signal for typical ambient mixing ratios (near 2ppm)? Moreover, the Allan-Werle plot for the in-flight operation uses ambient measurements; how do the authors assure that there are no atmospheric changes in mixing ratio during this UAV flight period? Was this timeseries measured during similar movements of the UAV than during the A and B field missions, or was it at a fixed location? How was the wind velocity, pressure, etc.?

We agree with the reviewer that laboratory performance does not always reflect performance in the field. We have made significant changes to the manuscript in an effort to characterize the instrument response when subjected to variations in temperature, pressure, humidity, and air flow. Those changes include a new subsection in Results titled: "3.2 Sensitivity to changing environmental conditions," which presents laboratory experiments in which the temperature and humidity were varied over time and for different methane mole fractions. We have also added a new subsection "3.3.3 In-flight stability and performance," which discusses how the background methane mole fraction varies over time during a flight. In the new Fig. 11, (see below) we have plotted timeseries data for the methane background, 2f peak and trough positions, altitude, temperature, pressure, relative humidity, ground speed, yaw, pitch, roll, wind speed, and wind direction. We show that most of the baseline drift occurs during takeoff and landing (up to 5% variation), but the maximum drift observed while executing the curtain flight pattern is 2.5%.

Regarding the Allan-Werle plot (Fig. 4, revised version below), the in-flight timeseries data has now been corrected to account for the effect of water vapor and to add reference lines for $\sqrt{1/\tau}$ white noise. We have removed the "ambient" qualification from the figure caption and related text to improve clarity.

As explained in the text, the laboratory test was performed under constant flow from a 2.00 ppm methane-in-air calibration gas cylinder. The in-flight test used a section of field data that recorded only background methane and the in-flight test duration was limited to 5 minutes to mitigate the potential impact of changes in the atmospheric mixing ratio over time. The flight pattern was similar to the curtain flight in controlled-release A, including abrupt changes in the flight altitude between 0 and 30 m above ground level. Information about the flight pattern and environmental conditions have now been added in the text:

L. 335-338: "The UAV flew a "curtain-type" flight pattern with horizontal transects at altitudes ranging from 0 to 30 m above ground level. The average wind speed during the flight period was 2.5 m s^{-1} with a standard deviation of 0.7 m s^{-1}. The temperature was around 22.5 °C, the pressure at ground level was 1005 hPa, and the relative humidity was 65%."

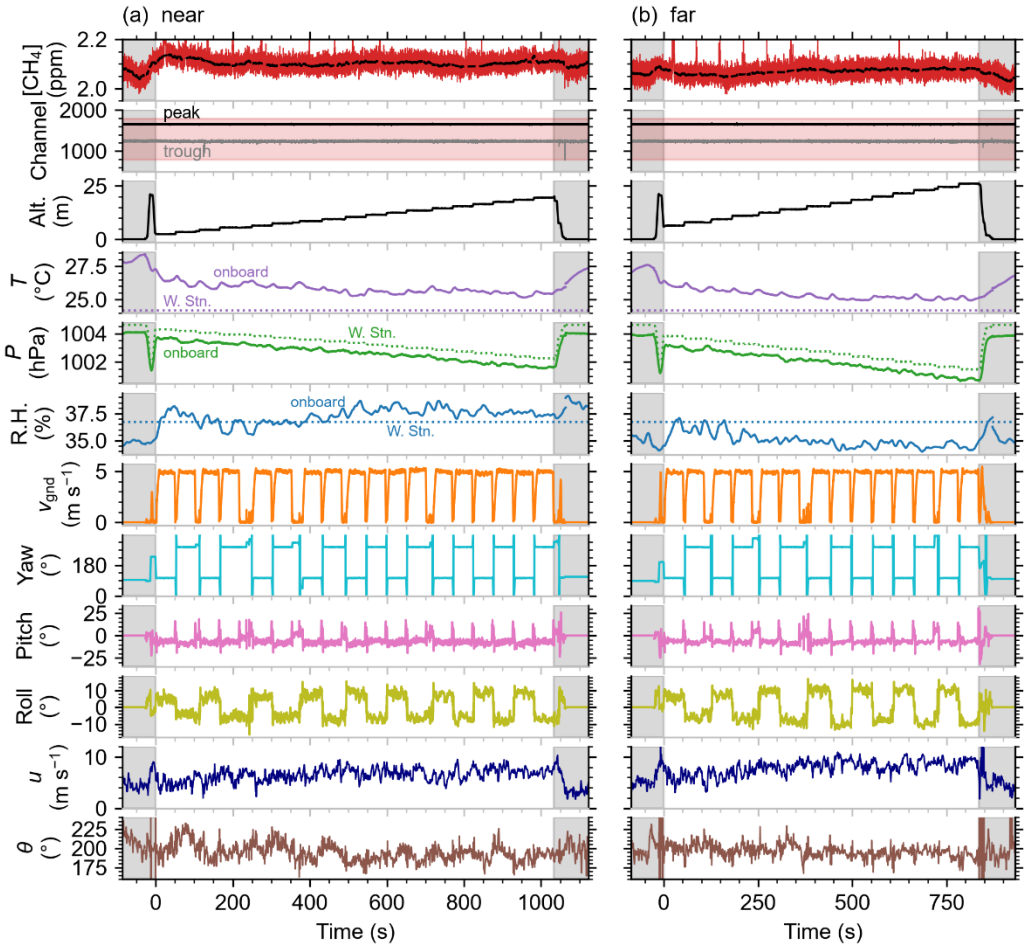

Figure 11. *Collection of parameters recorded over time for controlled-release (a) near and (b) far curtain flights. In order from top to bottom, the parameters are: methane mole fraction, 2f peak and trough channel numbers, altitude (Alt.), temperature (T), pressure (P), relative humidity (R.H.), ground speed (vgnd), heading (yaw), pitch, roll, wind speed (u), and wind direction (θ). The gray shaded bars at the beginning and end of each timeseries indicate data that falls outside of the defined flux curtain, including UAV takeoff and landing. The methane mole fraction scale is adjusted to emphasize the slowly varying baseline, displaying both the 10 Hz time series and the 5.8-second moving average of the background (black dashed line). The red shaded region in the peak and trough channel plot indicates the search bounds defined in Fig. 2. T, P, and R.H. measurements are shown for both the onboard sensor (10-second moving average) and average values from a local weather station (W. Stn.). Wind speed and direction were from the onboard anemometer.*

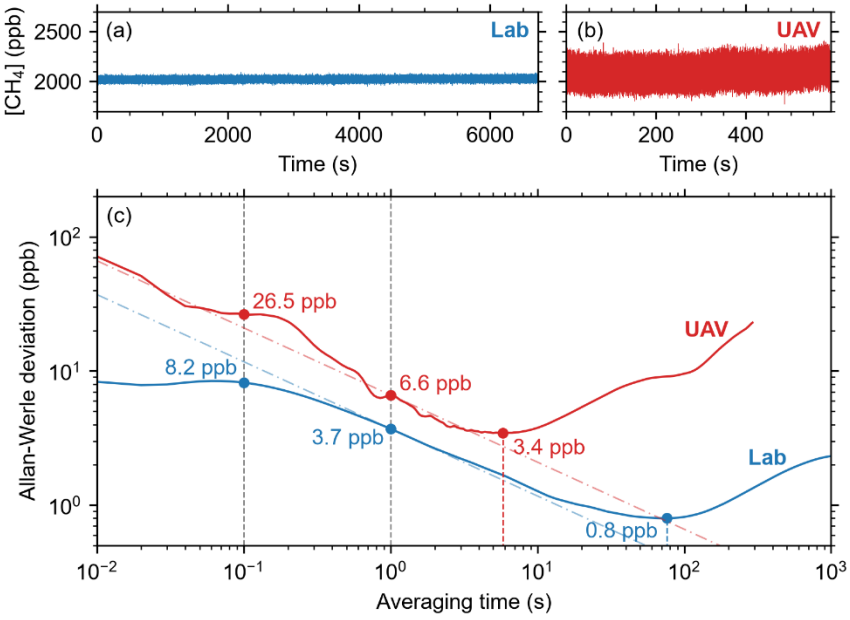

Figure 4. *(a), (b) Methane mole fraction 100 Hz timeseries (a) in laboratory enclosure and (b) during UAV flight. (c) Overlapping Allan-Werle deviation plots generated from the laboratory and in-flight timeseries. Dash-dot lines indicate* $\sqrt{1/\tau}$ *white noise behavior where τ is the averaging time (Werle, 2011).*

We have also expanded the discussion of the optimal averaging times. The new and revised text is below:

L. 345-362: "The in-lab Allan-Werle deviation below 0.1 s averaging time is affected by a quasi-periodic noise signature for which averaging does not initially improve the measurement precision, appearing as random-walk or correlated noise in the Allan-Werle plot. Though the root cause is still under investigation, the effect is likely induced by correlated mechanical or electrical noise (Röder et al., 2024; Gan et al., 2026). For the in-flight data, there is a deviation from the $\sqrt{1/\tau}$ white noise behavior observed for averaging times between 0.1 and 1 s that may be due to optical fringe effects that are not observed in the laboratory data (Werle, 2011)."

The Allan-Werle plot demonstrates that, by averaging the sensor's in-flight and laboratory mole fraction data up to 5.8 s and 75.9 s, respectively, corresponding optimum precisions of 3.4 ppb and 0.8 ppb are achieved. In both cases, sensor drift dominates precision beyond the optimal averaging times. In the laboratory, the test was performed in a temperature-controlled calibration enclosure, but gradual changes in pressure likely contributed to the drift. For the in-flight test, environmental conditions were not controlled and the sensor experienced rapid changes in air flow as the UAV changed directions. As a result, drift dominates the sensor behavior at shorter averaging times during flight compared with laboratory conditions."

The 1 s averaging times (in-flight precision: 6.6 ppb; laboratory precision: 3.7 ppb) represent a useful metric for comparison to other lightweight UAV sensors. Though other instruments offer slightly smaller 1 s precisions in the range of 1-5 ppb, to our knowledge the ultra-lightweight sensor presented here offers the best 1 s precision for a sub-2 kg methane sensor reported to date. For an open-path system on a mobile platform moving at 5 to 8 m s^{-1}, longer averaging times (>1 s) can result in smearing and loss of information. The averaging time that we use in this study is 0.1 s, corresponding to an in-flight precision of 26.5 ppb."

We have also added a more detailed discussion of how the instrument precision and drift contribute to the methane mole fraction uncertainty. This is discussed in the new section "3.3.3 In-flight stability and performance":

L. 532-539: "The in-flight measurements are used in tandem with results from laboratory experiments to estimate uncertainty on the methane mole fraction. The statistical component of the methane calibration error is set to 3%. This is a conservative estimate that accounts for the 1σ calibration uncertainty (<1.5%) and in-flight measurement drift (<2.5%). Measurement precision is also considered in the statistical error analysis, contributing 26.5 ppb for a 0.1 s averaging time and 3.4 ppb for the optimal 5.8 s averaging time used when analyzing the slowly varying background signal. Additionally, though the measured data was corrected to compensate for the difference in temperature and humidity compared to calibration, uncertainty in the correction factors and in the environmental conditions remains. For this reason, we apply a conservative systematic uncertainty of 5% in addition to the statistical uncertainty."

The full error propagation is discussed in the new "Appendix A: Uncertainty analysis for emission flux quantification".

> Particularly in mid-infrared absorption spectroscopy, frequent fringe or etalon structures contribute to the signal uncertainty. How sensitive is the sensor to those error contributions, along with contributions from changing pressure, temperature, and water vapor?

We thank the reviewer for their comment and question regarding the performance and sensitivity of the sensor to etalons, changing temperature, pressure, and water vapor. As mentioned above, the sensor's response to changing environmental conditions is discussed in the new sections "3.2 Sensitivity to changing environmental conditions" and "3.3.3 In-flight stability and performance". These results are inclusive of any etalon-induced uncertainties. We have updated the uncertainty estimates due to these environmental changes and included those in the uncertainty analysis section in Appendix A.

We agree that the quality of an infrared absorption spectrometer can suffer from parasitic fringes that may not be possible to eliminate entirely. However, the severity and sensitivity of a system to etalons, and their impacts on extracted information from spectral data is system-specific and depends on a few factors including optical design, and detection scheme, as also stated in Werle (2011). The use of transmissive optics with parallel or near-parallel surfaces makes a system more prone to etalon effects. In the present work we have attempted to mitigate etalon effects by using reflective optics, that is, an off-axis parabolic mirror for focusing of the light and mirrors with off-centre holes for coupling of the laser light in/out of the sample cell. In addition, here we employ wavelength modulation spectroscopy with second harmonic detection (*2f*-WMS) where a lock-in amplifier with a narrow bandwidth suppresses contributions from frequencies other than the demodulation frequency.

Although we have not separately studied the effects of etalons in the presented sensor and their associated uncertainties, to elucidate on the state of etalons in the present system, we performed a wavelength sweep of the laser by applying a ramp to the laser with no sinusoidal modulation. Figure R1 (below) shows the photodetector signal (left panels) and the corresponding signal in frequency domain (right panel). The modulation waveform was turned off in this scan to avoid over-crowding the frequency-

domain plot and to highlight etalons. Though this improves clarity, we acknowledge that potential etalons induced by the modulation waveform due to sum and difference frequency mixing would not be visible here.

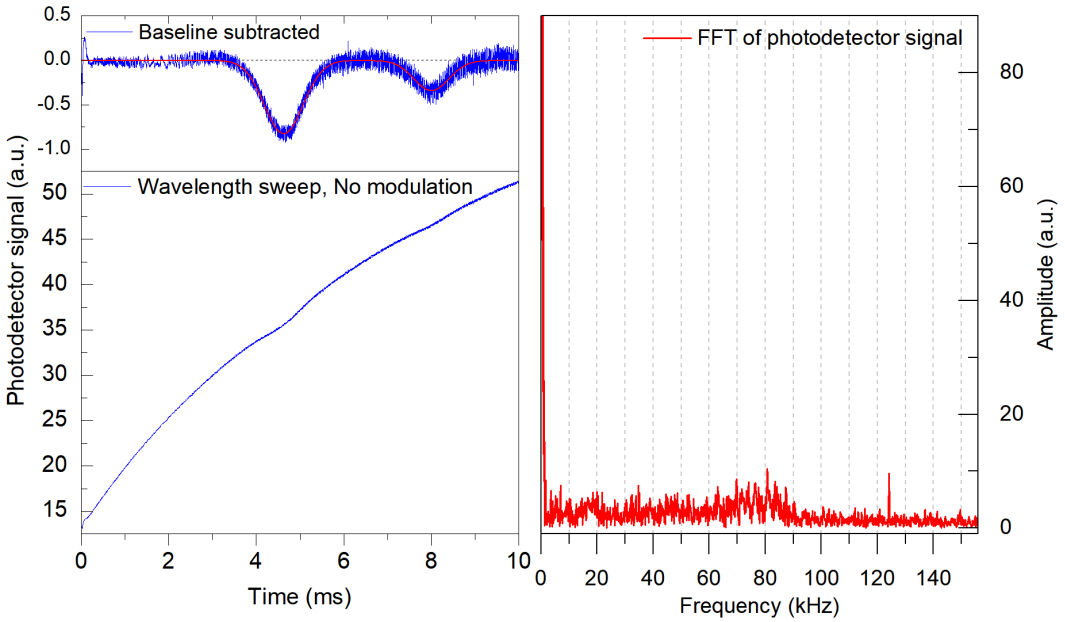

Figure R1. *Bottom left: Sample photodetector signal as recorded by the sensor's data acquisition system when the laser was driven with only a ramp waveform. Top left: Baseline subtracted spectrum of the bottom left panel. Right: One-sided fast Fourier transform spectrum of the photodetector signal computed with a Hanning window.*

In the frequency domain (right panel), the most significant features are in the range of 60 to 90 kHz. These features are attributable to etalons, and these are the components that make up the Y-spread of the signal seen in the top left panel (baseline subtracted). Etalons also appear below 60 kHz due to the non-linear tuning behaviour of the laser (see, e.g. chirping etalons around 2 ms). Therefore, the most significant etalons do not appear close to the modulation frequency (10 kHz) or its second harmonic (20 kHz), which would directly pass through the lock-in amplifier and contaminate the desired signals heavily. As discussed in Werle 2011, etalons with free spectral range (FSR) that appear as high frequency components (relative to the modulation frequency) are relatively easily handled by low-pass filtering, e.g. in a lock-in amplifier when performing WMS. In contrast, etalons with FSR comparable to the linewidth of the target absorption feature and those with broad structures can have a larger effect on weak absorption signals. No etalons with FSR comparable to the absorption linewidth are observed in the baseline-subtracted spectrum (top left panel). Etalons with broad structures impact the baseline and are more difficult, or impossible, to observe in a direct absorption signal or its frequency-domain counterpart, since they appear as very low frequencies. These etalons can pass through the lock-in amplifier, resulting in distortion of the absorption features or contributing to baseline values either directly or indirectly via non-linear mixing with the modulation frequency.

We have also investigated the frequency components in the 2*f* spectrum that is used for mole fraction determination. The bottom left panel of Figure R2 shows a sample X_{2f} spectrum. The top left panel shows a portion of the spectrum magnified by ~150 times on a flat region of the baseline to show the residual periodic signals. We notice that this periodic signal has a frequency equal to the modulation frequency (10 kHz) and attribute it to residual intensity modulation due to the non-ideal performance of the lock-in amplifier low-pass filter. As can be seen in the right panel, this component has an amplitude about 60 dB lower than the low-pass filtered signal, i.e. X_{2f}, with higher harmonics decreasing in amplitude. In our assessment, these ripples, whether from residual intensity modulation or non-linear mixing of modulation with etalons, do not impact the consistency of the X_{2f} spectrum over time. However, they could affect the value of the peak-to-trough metric, used for mole fraction retrieval, in the peak-finding algorithm via detection of adjacent ripple peaks. We have included in the new Fig. 11, found in Section 3.2.3, peak and trough locations recorded by the sensor during flight.

In general, the presented results in this paper on the sensor performance characteristics are inclusive of the etalon effects that impact the final reading of the sensor.

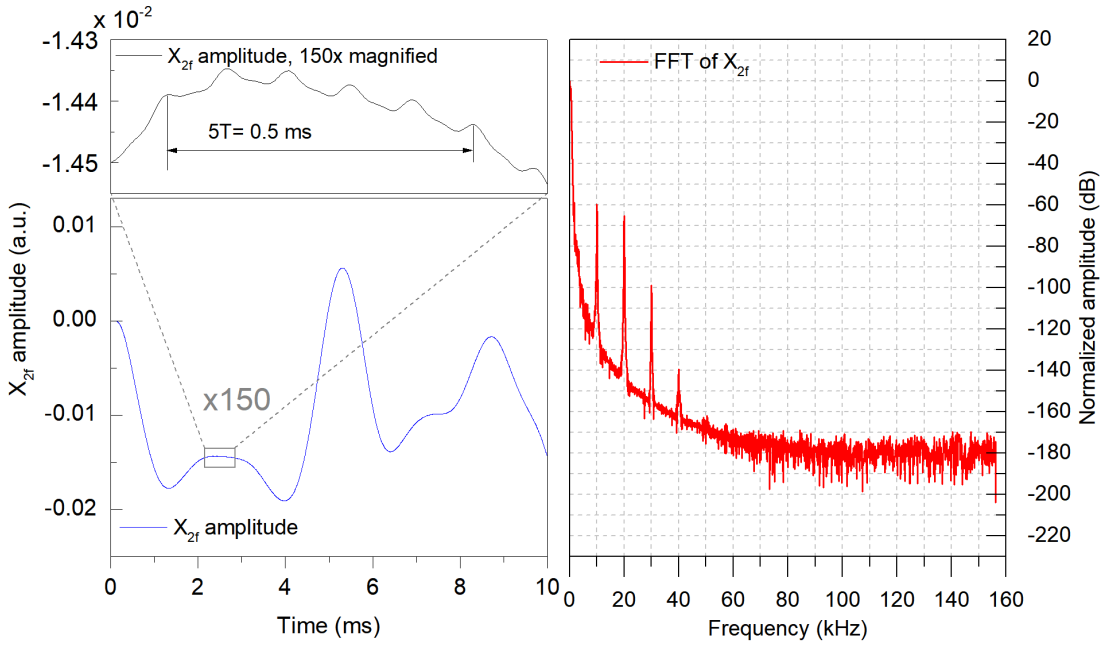

Figure R2. *Bottom left: a sample X_{2f} spectrum. Top left: magnified portion of X_{2f} around the flat baseline region to show residual periodic signals riding on the X_{2f} signal. Right: fast Fourier transform spectrum of X_{2f} spectrum, computed with a Hanning window.*

How do the authors justify to use a 1 Hz time resolution, where they only are able to detect atmospheric methane variabilities with a precision of 26 ppb. Moreover, total measurement uncertainty can not only be explained by the precision, particularly when the standard deviations of the timeseries in the lab and during flight in Figure 4a,b seems to be at +-50 ppb and +-250 ppb, respectively. According to the Allan-Werle deviation at 100 Hz resolution, this cannot fully be explained by precisions of approx. 8 ppb, and 70 ppb, for lab and in-flight respectively. How do the timeseries look like with the optimum averaging times? What is the total uncertainty predicted for the ambient observations, e.g., including drift, reproducibility, etc.?

We thank the reviewer for this question about the precision. The standard deviations (σ) over the entire 100 Hz timeseries shown in Fig. 4 are 14.7 ppb and 74.8 ppb for the laboratory and in-flight datasets, respectively. Figure R3 below shows the timeseries datasets with horizontal lines indicating the mean, the 1σ and 2σ bounds. For the laboratory data, the 100 Hz standard deviation of 14.7 ppb is larger than the Allan-Werle deviation at 0.01 s (8.3 ppb) because the simple standard deviation calculation does not distinguish correlated noise that appears in the Allan-Werle plot. For the in-flight data, the standard deviation of 74.8 ppb is very similar to the Allan-Werle deviation of 71.3 ppb. The asymmetrical distribution of the 100 Hz in-flight timeseries data is induced by signal drift and by additional sources of noise that are not present in the laboratory dataset, such as inductive noise from radio transmission.

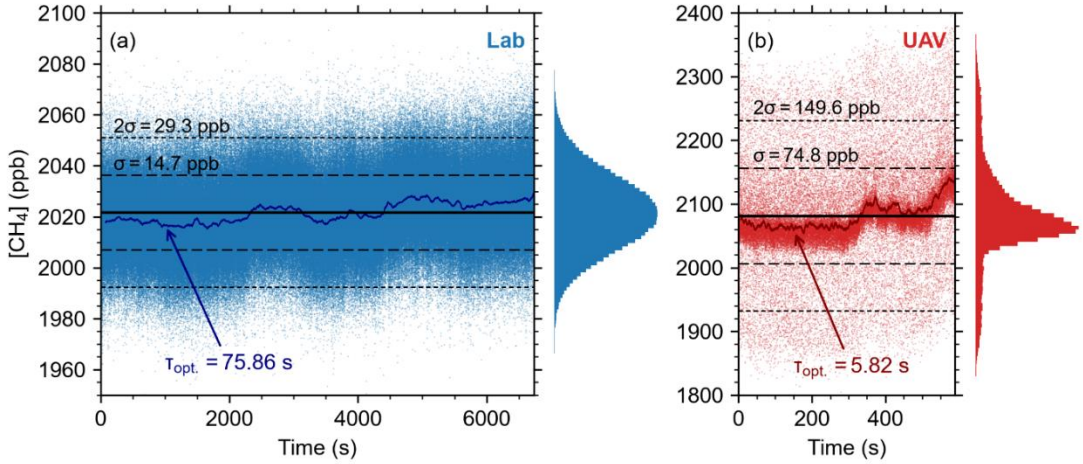

Figure R3. *100 Hz timeseries for (a) lab and (b) in-flight datasets – equivalent to Figure 4. Horizontal lines indicate the mean and the 1σ and 2σ bounds. The histograms show how the data is distributed. Timeseries datasets reflecting optimal averaging times of 75.86 s (lab) and 5.82 s (UAV) are also indicated.*

Figure R3 also shows the timeseries datasets reflecting optimal averaging times ($\tau_{opt.}$) for both laboratory and in-flight tests. The 10 Hz time resolution implemented in-flight, which is associated with a precision of 26.5 ppb, was chosen to balance sensor precision with spatial resolution. Longer averaging times near the optimal value of 5.82 s are suitable for monitoring the slowly varying signal baseline and are therefore used in the background subtraction, as described in the new "Section 3.3.2 Background subtraction". However, for rapid variations in the methane mole fraction observed when transecting the plume from a nearby point source, shorter timescales are needed to create a detailed plume map and avoid excessive smoothing of the data, which may obscure peaks. For a UAV platform that is traveling at 5 m s^{-1}, the intrinsic 100 Hz timeseries dataset is associated with a spatial resolution of 0.05 m. In the case of controlled-release A, most of the recorded peaks have a width of roughly 10 to 20 m. Averaging to the "optimal" value of 5.82 s would smear the data over a spatial distance of 29 m, which is therefore unsuitable. Averaging to 0.1 s results in a more appropriate spatial resolution of 0.5 m. In the corresponding 10 Hz timeseries dataset for controlled-release A, the height of the smallest recorded peak is roughly 150 ppm, which is a factor of six larger than the 10 Hz measurement precision, large enough to be clearly distinguishable.

As stated above, total uncertainties are discussed in detail in Appendix A.

> The instrument performance and possible atmospheric applications need to be put into better context, and clarified, for which type of atmospheric methane sources the sensor can be used for (e.g., strong emitting sources such as oil/gas lacks, wastewater facilities (report corresponding literature)). I miss the statement how this controlled-released field campaigns are satisfied to represent real-emission scenarios. While the intentional release of a potent greenhouse gas at fluxes of approximately 0.5 kg h^{-1} should be considered carefully, the study would benefit from an additional in-field characterization experiment. In particular, a comparison with simultaneous measurements from an independent ground-based instrument (e.g., Aeris Pico, MIRA Pico deployed on a tower or mobile platform) at a real methane emission source would help to better quantify the performance of the airborne sensor. Such an experiment would also provide a clearer demonstration of the system's potential applicability for future in-field measurement campaigns.

We thank the reviewer for their insightful comments. Though we have not rigorously evaluated the lower limit of emissions that can be reliably quantified by the method presented here, the sensing platform in its current configuration is likely best-suited to measure emissions from point sources with emission rates $\gtrsim$ 0.4 kg h^{-1}. Such emission sources are common in small oil and gas facilities. For even smaller sources, mitigating in-flight noise would improve the capability of the instrument, and repeated flights would increase the probability of detection. Flying the UAV at a slower ground speed and increasing the averaging time could also enable quantification of smaller sources, though it would reduce the number of transects that can be collected over a single flight due to limitations of the UAV battery. On the other hand, for large emission sources (~100 kg h^{-1}) it may be necessary to deploy the instrument farther downwind or to install a multi-pass cell with a shorter path length to avoid the instrument's saturation regime. For reference, just 1% of the laser light will be transmitted when the methane mole fraction reaches 200 ppm for the 4.6 m multi-pass optical cell reported here.

Sources that are known to emit methane in a suitable range for this instrument include oil and gas facilities such as well sites, compressor stations, or gas processing plants (Donahue et al., 2026), wastewater treatment facilities (Gillespie et al., 2025), small landfills (Dooley et al., 2025; Gillespie et al.), and naturally occurring geologic gas seeps (Bolek et al., 2026). The controlled release studies presented in this work most closely resemble leaks from small oil and gas facilities where a fugitive emission source is located just a few meters off of the ground.

Deployment to measure real methane emission sources is ongoing parallel work. We have a second manuscript in which we present measurements of emissions from a naturally occurring geologic methane seep, including a comparison to the commercially available Aeris MIRA Strato sensor deployed on a second UAV system. That manuscript was concurrently under review and was recently accepted for publication in AMT (Bolek et al., 2026). As shown in that work, emission rate estimates were similar for both sensing platforms, on the order of 10 kg h^{-1}, demonstrating our sensor's suitability to characterize emissions from point sources. It should be noted that other natural sources of methane emissions associated with slow changes of methane concentration in their vicinity, such as wetlands and peatlands, are not the target application for the sensor and UAV platform reported here, in its current configuration.

> The spectra in Figure 2 shows the absorption lines of CH4 and H2O for roughly 2ppm of CH4, right? The 2f spectrum is usually ideal to define a background line, with usually no absorption if there is no error contribution. If I understood it correctly, methane mixing ratios are computed by a peak-to-peak amplitude searching the minimum and the maximum signal within predefined bounds. That would work if the background line would not experience etalon or other sinusoidal structures, which it seems to experience, as it looks like in Figure 2c, and the Allan-Werle plot. Those structures would non-linearly expand (or decrease) the peak-to-peak amplitude, resulting in much higher (or lower) mixing ratios than existing. Have the authors tried to use an average background line instead of a minimum peak? What are the predefined bounds to compute

the peak-to-peak amplitude? How much does the signal drift during operation, as no line-locking or calibration is done to identify the correct absorption line? How can it be assured that the H2O line does not lie within the predefined bounds at some point?

That is correct, the methane mole fraction for Fig. 2(b,c) is roughly 2 ppm. We have updated Fig. 2(c) to show the predefined bounds used for finding the peak and trough of the methane absorption feature for the peak-to-peak metric (could also be called, peak-to-trough). Sinusoidal structures present in the demodulated spectrum are not visible in (c). Such figures are depicted in Figure R2 by magnifying the vertical scale by ~150 times. Though these small structures do degrade the signal quality in the form of decreased precision compared to a pristine baseline, they are reflected in the sensor performance metrics.

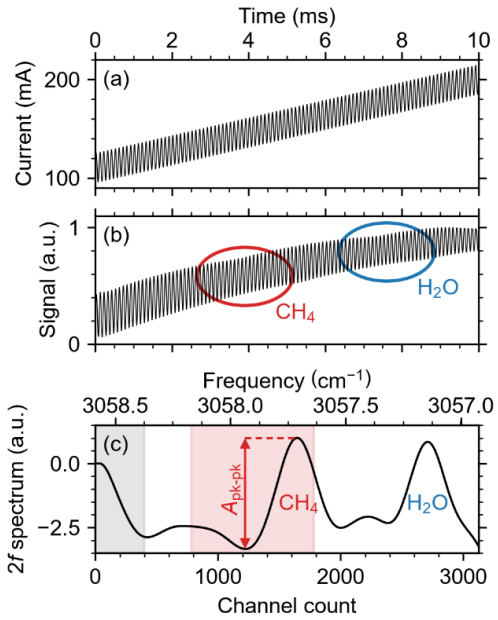

Figure 2. *(a) Laser injection current ramp and 10 kHz modulation over one sawtooth period. (b) Corresponding normalized detector signal observed under ambient measurement conditions. (c) Demodulated second harmonic spectrum, normalized. Absorption features due to CH_4 and H_2O are indicated in (b, c). The gray shaded region in (c) spanning channels 0 to 400 contains the initial response of the low pass filter and does not indicate absorption. The red shaded region covering the CH_4 peak indicates the predefined bounds used to identify the peak-to-peak amplitude.*

Though we do not use line locking, the laser temperature is very well controlled and the position of the methane absorption feature is confirmed in the laboratory using a CH_4 low pressure cell. We have added a new subsection "3.3.3 In-flight stability and performance" containing the new Fig. 11, which shows how the background methane mole fraction varies over time during a flight. Along with the methane background, we have plotted timeseries data for the 2*f* peak and trough positions, which in general shift by <1.5% of the total scan range. From the stability of the peak and trough positions and given that the methane and water peaks maintain a constant spectral shift (35% of the scan range), we know that the water peak does not migrate to within the methane peak search bounds.

Though we have experimented with alternative baseline extraction methods for other WMS sensors, for the compact, ultra-light instrument presented in this work we have exclusively relied on the peak-to-peak metric. The primary reason for this has been to take advantage of the method's simplicity and avoid additional computational steps for the sensor's onboard SBC.

Throughout the manuscript several different time resolutions, and precisions are reported. For example, in the Abstract, the authors state a precision of 3.7 ppb at 1 s time resolution; but in the field missions they use an averaging time of 0.1 s with a reported precision of 26 ppb. Please decide which resolution and precision is appropriate for the sensor and assure continuity throughout the manuscript.

As discussed above, the most appropriate averaging time depends on the deployment conditions and the overall objective. This is why different averaging times are used for the background signal and the elevated signal in the background subtraction procedure, described in Section 3.3.2. We feel that the 1 Hz precision is a useful metric for comparing to other sensors, for which precision is often reported at 1 Hz. However, we agree with the reviewer that improved clarity is required. We have modified the abstract as follows:

L. 10-12: "The measurement precision for a 1 s averaging time is 3.7 ppb in the laboratory and 6.6 ppb in-flight. The 0.1 s in-flight precision, which is more suitable for monitoring rapidly varying methane from a fast-moving platform, is 26.5 ppb."

We also modified the relevant text in the conclusion:

L. 595-600: “The sensor achieves an in-flight precision of 6.6 ppb at 1 Hz which, to our knowledge, is the best 1 Hz precision for a UAV-borne methane sensor weighing less than 2 kg reported to date. The in-flight precision could be further improved by mitigating inductive noise produced by the sensor’s on-board radio, used for real-time data streaming. Laboratory measurements without real-time data streaming show a 1 Hz precision of 3.7 ppb. When deployed on a fast-moving UAV platform traveling at 5-8 m s^{-1}, a 10 Hz time resolution is used for signal averaging, corresponding to an in-flight measurement precision of 26.5 ppb.”

In-line comments:

Abstract:

In the abstract, the key findings of this manuscript should be briefly reported and motivated. What is the motivation? What are the key aspects of the sensor (not necessarily need to report the electrical power)? And what test have been done to evaluate the instrumental performance?

We thank the reviewer for their suggestions. The revised abstract is below:

L. 1-16: “Uncrewed aerial vehicles (UAVs) offer versatile platforms for low-altitude (1 to 120 m) trace-gas measurements that can fill spatio-temporal measurement gaps between ground-based mobile platforms and conventional aircraft measurements. Small UAVs (under 25 kg) are easier to transport and typically face fewer regulatory restrictions than larger ones. However, they have significant payload limitations, underscoring the importance of developing lightweight, high-performance gas sensors for UAV deployment. In this work, we developed an ultra-lightweight methane sensor based on mid-infrared spectroscopy for precise, rapid in-situ measurements aboard small UAVs. Weighing just 1.2 kg, including the dedicated battery, the stand-alone, power efficient instrument is 75% lighter than our previous design, making it one of the lightest methane sensors reported to date. The design is simple and compact, featuring a Herriott-type multi-pass cell in an open-path configuration. We report the sensor performance in detail in both laboratory experiments and field deployments, including the response to variable environmental conditions. The measurement precision for a 1 s averaging time is 3.7 ppb in the laboratory and 6.6 ppb in-flight. The 0.1 s in-flight precision, which is more suitable for monitoring rapidly varying methane from a fast-moving platform, is 26.5 ppb. We deployed the sensor in a controlled-release experiment with a methane point source emitting 0.48 kg h^{-1}. Using a direct mass balance flux quantification approach and wind measurements recorded by an on-board anemometer, estimated emissions were within 9% of the true emission rate. The results demonstrate the instrument’s potential for in-situ measurement of fugitive emissions from anthropogenic and natural point sources. Further systematic controlled-release studies are needed to fully assess the detection probability and quantification accuracy of this UAV-based measurement system.”

Line 1: change “mobile” into “in-situ”

The revised sentence reads:

L. 6: “…precise, rapid in-situ measurements aboard small UAVs.”

Lines 8-9: “undetectable for other methods”? This is a strong statement, and not true. Balloon-based or flux-tower based measurements, e.g., also provide such low-altitude in-situ data.

The revised sentence reads:

L. 14-15: “The results demonstrate the instrument’s potential for in-situ measurement of fugitive emissions from anthropogenic and natural point sources.”

Introduction:

The introduction generally needs more literature citations. There are a lot of facts stated without referring literature to it (e.g., line 18, 24, 30).

We have added more citations to the introduction, including citations to support the examples highlighted by the reviewer, as shown in the excerpts below:

L. 24-26: “Vehicle-based mobile surveys are generally restricted to the route of travel (e.g., roadways, pathways, water channels, etc.) and provide information about a gaseous plume only at a single height, typically < 3 m above the ground (Caulton et al., 2018; Kumar et al., 2021; Tettenborn et al., 2025).”

L. 32-37: “Conversely, crewed aircraft have minimum safe flight altitudes that are typically > 100 m above ground level and depend on a number of factors, including the terrain, aircraft, and specific flight conditions. For reference, in Canada the minimum flight altitude is 500 feet (152 m) above the highest obstacle in rural environments, or 1000 feet (305 m) in built-up areas

(Canadian Aviation Regulations, SOR96/433, s602.14, Government of Canada (2026)). As such, crewed aircraft surveys often do not capture the full vertical extent of a plume close to the surface, requiring extrapolation over hundreds of meters between the lowest flight altitude and the ground."

L. 41-42: "For this reason, extremely stable and sensitive instruments are required to distinguish changes in gas mole fractions from instrument drift (Röder et al,. 2024)."

Line 12: Change "processes" into "sources"

The revised sentence reads:

L. 19: "…from both anthropogenic and natural sources…"

Line 13-16: What about flux towers?

We thank the reviewer for their comment. Though flux towers are a commonly used in-situ measurement technique, our intention was to focus on comparison to mobile measurement platforms. To clarify this intention, we have revised the sentence to read:

L. 20-21: "Until recently, technologies for in-situ mobile measurement surveys of surface-based emissions were primarily limited to ..."

Add a comma after "e.g."

This has been corrected.

Line 24-25: ">100 m" or "hundreds of meters"? It really depends here on the terrain and aircraft. Over the ocean a small aircraft can fly even lower than 100m. Maybe it would be better to emphasize the requirements of extrapolation, if difficult terrain and vegetation are present.

We have clarified the text to emphasize that the limits depend on the scenario, citing Canadian regulations. The revised text (L. 32-37) can be found on the previous page of this response letter.

Line 28: "greater distances" are also a huge benefit of aircraft observations, as those allow air parcel tracking or convective plume tracking for smaller up to longer distances (see Karion et al., 2015, Conley et al., 2017, Riese et al., 2025, Curtius et al., 2024)

We agree with the Reviewer that aircraft surveys have advantages over other technologies for certain applications. We have therefore revised the text to emphasize the differences with drone-based surveys:

L. 39-44: "Consequently, crewed aircraft measurements must be performed at much greater distances from the emission source than is required for ground-based measurements. Dispersion and dilution over these distances results in lower methane mole fractions at the detection location and a lower probability of detection. For this reason, extremely stable and sensitive instruments are required to distinguish changes in gas mole fractions from instrument drift (Roder et al., 2024). As a result, aircraft-based methane surveys are generally best suited to characterizing sources with emission rates > 10 kg h^{-1} (El Abbadi et al., 2024; Duren et al., 2019), though 90% probability of detection thresholds have been demonstrated for emission rates as low as 1 kg h^{-1} (Donahue et al., 2026)."

Line 30 – 31: "extremely stable and sensitive instruments" also exist particularly built for aircraft in-situ observations (see, e.g., D'Amato et al., 2025, Ort et al., 2024, Müller et al., 2015, Viciani et al., 2018)

We agree with the Reviewer that stable and sensitive instruments have been developed and deployed very successfully on crewed aircraft for in-situ observations. See response to previous comment for the revision that further clarifies this section of the text. However, extremely stable and sensitive instruments often have higher weight and power consumption, which does not meet the payload requirements of small UAVs.

Lines 41-55: This comparison between "in-situ" and "ex-situ" (while the phrasing "remote-sensed" is more commonly used in atmospheric measurement techniques) is a bit out of context here. I see the point of motivating in-situ over remote-sensed techniques here, but maybe shortening this part and may expanding on comparisons between more similar drone sensors instead would highlight the benefits of the reported sensor more.

We thank the Reviewer for the suggestions. The discussion of in-situ vs. remote sensing has been condensed and now reads:

L. 59-66: “In remote sensing, column-integrated gas concentrations are inferred from surface-scattered light or thermal emissions, usually detected from the aerial platform. Remote sensing offers broad spatial coverage and rapid plume mapping, ideal for large-scale surveys and locating emission hot spots, but detection limits depend on flight altitude and ground surface properties, as well as meteorological conditions. In contrast, in-situ instruments measure gas within a specified sampling cell, detecting small concentration enhancements that would be undetectable by remote sensing methods. In-situ methods are well-suited to ground truthing, targeted detection of small methane enhancements, and deployment over surfaces that are challenging or unsuitable for instruments that rely on surface-scattered light, such as water or wetlands.”

We have also expanded the comparison to other similar UAV sensors, as described on page 1 of this response letter.

> Line 58: “a delayed response”: this depends on the pump and flow rate used in the system. Clarify more what you mean, add more citation.

We thank the Reviewer for their comment. We have revised the text to explain this point more clearly:

L. 68-71: “The sampling cell is protected from the environment, but exchange rates and mixing within the cell cause a delayed response and can change the shape of the plume recorded from a mobile platform, leading to potential underestimation of the true gas enhancements (Takriti et al., 2021; Tettenborn et al., 2025; Maazallahi et al., 2023).”

> Line 62-64: It may be helpful here to clarify more which limitations and challenges exist for open-path systems and how your system is trying to tackle those.

We have expanded on the discussion of the limitations of open-path systems, as described below:

L. 74-79: “However, optical elements exposed to the environment require more frequent maintenance. This adds to the complexity and challenge of long-unattended deployments of open-path systems (McDermitt et al., 2011), but does not cause operational limitations when deploying on UAVs with short flight times. Open-path instruments are also directly exposed to environmental conditions including variable temperature and pressure, which can affect the sensor behavior, though the variability of conditions is less drastic for a UAV-borne sensor than for sensors deployed on aircraft flying hundreds of meters above the ground (D’Amoto et al., 2025).”

L. 126-127: “We present the instrument’s laboratory and field performance when deployed on a small enterprise-grade UAV, and evaluate the impact of variable environmental conditions.”

> Line 65: weird sentence structure: “deployed for deployment”

The sentence (L. 108 in revised manuscript) reads: “<u>developed</u> for deployment.”

> Line 67 (& line 84): Where do you define v3? Do you need it anywhere again?

ν_3 refers to the methane vibrational mode that we probe with absorption spectroscopy in this work. We have now defined the mode more clearly:

L. 100-101: “For methane, however, the strongest absorbance is found in the ν_3 fundamental C-H stretching mode near 3.3 µm (Dang-Nhu et al., 1979), …”

> Line 65-75: Sounds more like a conclusion. Maybe combining it with the part in line 76-80 and shorten it would help.

We have made substantial changes to the text in this section, removing some details that are explained in later sections and moving other text to the conclusion. The revised text is below:

L. 108-129: “In this paper, we present an ultra-lightweight open-path laser spectroscopic methane sensor that we developed for deployment on small UAVs. Similar to an earlier prototype (Norooz Oliaee et al., 2022), the sensor is based on mid-infrared (mid-IR) TDLAS. The laser wavelength is tuned across methane's strong ν_3 fundamental absorption mode, enabling high-precision measurements. Compared to its predecessor, the new instrument is substantially smaller, lighter, and more power efficient, achieving a unique combination of high performance with an ultra-lightweight, compact design. This improvement could facilitate the widespread adoption and deployment of rapid-response laser-based gas sensors on small UAVs and other suitable platforms.

The methane mole fraction is inferred using WMS. Unlike DAS, in which the gas mole fraction is determined directly from the transmission spectrum, in WMS the laser wavelength is swept across the molecular absorption line and modulated sinusoidally. Detection of the filtered and demodulated signal at harmonics of the modulation frequency enhances the signal-to-noise ratio and the measurement sensitivity as compared to DAS (Norooz Oliaee et al., 2022). The gas mole fraction is retrieved from the

amplitude of the corresponding peak in the second harmonic spectrum. Beyond improved signal-to-noise, the implementation of WMS is simpler than DAS and more easily adapted to the ultra-lightweight embedded platform with its onboard single board computer (SBC). Conversely, the more complicated DAS fitting algorithms require more computational resources than WMS, which may necessitate a more powerful SBC or the use of a ground station to process the spectral data (Tuzson et al., 2020).

Here we report the sensor architecture, including the compact and simple optical assembly, integrated electronics, SBC, and custom data acquisition board that have been instrumental in achieving a lightweight, power-efficient, and high-precision sensor with onboard data processing. We present the instrument's laboratory and field performance when deployed on a small enterprise-grade UAV, and evaluate the impact of variable environmental conditions. We also present a complete system for UAV mass-balance flux estimation including an on-board anemometer for wind measurements. The system's capacity to estimate emission rates from a methane point source is demonstrated in a controlled release experiment.

Line 71 & line 77: "SBC" is defined twice here. Once is enough.

The duplicate definition of SBC has been removed.

Section 2.1:

This section feels unnecessary, as it repeats your last part in the introduction and detailed descriptions to the principles that are explained anyhow in the following Sections. I would remove this part, include some of it into later sections, or motivate in the introduction. For example, why haven't you used DAS instead of WMS? Why TDLAS and not QCLAS, which is anyhow claimed to be more suitable for small and compact absorption spectrometers? This should be motivated more in the introduction.

We thank the reviewer for this suggestion. We have removed this subsection, moving most of the text either to the introduction or to other subsections under Methods. We have also expanded on the discussion of DAS vs. WMS (L. 115-123) and TDLAS vs. QCLAS (L. 97-107) in the introduction. The excerpts can be found on pages 1-2 and 11-12 of this response letter.

Section 2.2:

Include the temperature range of the laser

The temperature range has been added and the revised text reads:

L. 132-134: "We use a collimated GaSb-based distributed feedback (DFB) diode laser (NL3270-TL, Norcada, Canada) with a specified operating temperature range from -20 to 40 °C. The laser wavelength is 3270.4 nm at 7 °C when the injection current is 130 mA."

Line 90: Write "Figure", as it starts the sentence

"Fig." has been replaced by "Figure" at the beginning of all applicable sentences.

Line 92: What kind of Herriott cell exactly (spot-ring, astigmatic, etc.)? Add citation, accordingly.

We are using a spot-ring Herriott cell. This has been specified in the text and a citation has been added:

L. 135-136: "The laser light is launched into an open-path multi-pass spot-ring Herriott cell (Herriott et al., 1964), chosen for its simplicity and compatibility with commercial off-the-shelf mirrors."

Line 94, 95: Remove the brackets at the citation

Brackets around the textual citation have been removed.

Line 95: What is the reflectivity of the gold-coated mirrors? Please add.

Sentence has been added:

L. 140-141: "The reflectivity of the mirrors at 3270.4 nm is reported by the manufacturer to be 98.6% for a 10° angle of incidence."

Line 98: I think the authors confused the unit of the path length here. Within a multi-pass cell of length 131.4 mm and 35 passes, 4.6 km path length sounds a bit too much for me.

The path length is 4.6 m (not km). To avoid confusion, we have removed the trailing zeros and replaced "4.600 m" with "4.6 m".

Section 2.3:

Move Section 2.3. after Section 2.5. This would improve the flow as you would have explained all parts already, which are mentioned here.

The "Mechanical assembly" section (formerly 2.3) has been moved to come just after the "Onboard signal generation, acquisition, and processing" section, per the reviewer's recommendation.

Line 106: The optical alignment should be transferred into the Section "Optical assembly" and the alignment method should be described in more detail. How can shims achieve such fine injection angles? How was the correct adjustment approved? Did you use a visible light source for the adjustment? Was the cell itself already adjusted?

The text describing the optical alignment procedure has been revised and moved to the Optical Assembly section. The revised text reads:

L. 147-154: "The laser, its heat sink, both mirrors of the multi-pass cell, and the OAPM are integrated into a rigid, cage-like assembly that reduces the effects of mechanical vibrations during UAV flight deployments (see Fig. 1 (c)). Laser pre-alignment is achieved using a mounting plate machined at the desired injection angle. The optical alignment is fine-tuned during the assembly procedure using shims and split lock washers to correct deviations in the laser pointing angle. The split lock washers provide small angular adjustment capability, while slightly over-sized mounting holes for the laser heat sink and off-axis parabolic mirror allow limited translational freedom. Final alignment was achieved by measuring the laser pointing angle, applying the required corrections, and making small translational and angular adjustments to maximize the detector signal observed on an oscilloscope. The number and approximate positions of the reflected spots are confirmed by systematically blocking the laser beam."

Line 109: Clarify here again in brackets, which quantities the ambient condition sensors can measure.

The ambient condition sensors are now specified in brackets:

L. 220: "…ambient condition (pressure, temperature, and relative humidity) sensors…"

Section 2.4:

Explain how the cooling of the laser and detector works, and what the heatsinks are there for. How much varies the laser and detector temperature in field operation? And what's the range of impact on the signal with changing temperature?

We have revised the "Temperature control and power consumption" section to explain the laser and detector cooling in more detail:

L. 157-162: "Both the laser and the photodetector are temperature-stabilized via integrated thermoelectric coolers (TECs), controlled by ultra-stable TEC controllers (WTC32ND, Wavelength Electronics, USA). The laser is mounted on a custom aluminum heatsink affixed to the multi-pass optical cell. The photodetector is mounted directly to the sensor's aluminum baseplate, which also dissipates heat. The TEC controllers are mounted on custom-designed printed circuit boards (PCBs), which were adapted from the manufacturer's evaluation board (WTC32ND-EV, Wavelength Electronics, USA) with added fail-safe protection circuitry to prevent accidental thermal runaway events. Heatsinks affixed to the aluminum baseplate directly opposite the TEC controllers dissipate heat generated by the TEC drive currents."

We have also added the following sentence to describe the in-flight laser temperature stability and the associated impact on the laser wavelength:

L. 163-165: "Under active airflow, the temperatures of both laser and detector typically stabilize within 10 minutes. A similar stabilization period is required after rapid, substantial changes in ambient temperature. During UAV flight, the laser temperature is maintained to within ±0.1 °C, which corresponds to a wavelength stability of ±0.028 nm (±0.026 cm^{-1})."

This small temperature variation has a negligible impact on the methane 2*f* spectrum, as seen in the updated Fig. 2, which shows the bounds used in the peak-finding algorithm. The temperature of the photodetector was not monitored during flight – this will be the subject of future study.

Section 2.5:

Line 135: Add citation of the HITRAN line for the chosen methane absorption line.

References to the chosen absorption line have been added in the text:

L. 179-180: "…tuned to the methane absorption line at 3270.4 nm (Dang-Nhu et al., 1979; Gordon et al., 2026)."

> Line 141: Why 2f and not, e.g., direct absorption? Explain more the reasons for your choice. Include references of airborne instruments also using 2f (ALIAS, BLISS, DACOM, ATLAS, ATTILA).

We have expanded on the reasons for using WMS rather than DAS in the introduction (excerpt on page 11-12 of response letter). The introduction also makes reference to other lightweight sensors deployed on UAVs that use WMS (Nathan et al., 2015; Golston et al., 2017).

> Line 148: "section" to "Section"

The capitalization has been corrected.

> Section 2.6:
>
> Clarify better how long the UAV can be operated in field. Line 166 and line 184 report two different (maximum) flight times. Stick here to what is possible for full operation mode under ambient conditions, considering wind and temperature ranges. Adjust the maximum operation time also in the conclusions (line 355).

The methane sensor was designed as a standalone unit that could be deployed on various different UAV platforms, and it is powered independently from the UAV. In this manuscript, we document sensor deployment on the DJI M300, but we have separately deployed the sensor on another UAV that had different flight time limitations. We have revised the text to clarify the UAV flight times that we achieved with the DJI M300 and to highlight that the flight time is limited by the UAV batteries and not by the methane sensor. The revised text reads:

L. 228-231: "With the sensor onboard, we have achieved UAV flight times up to 28 minutes, limited by the UAV batteries. The methane sensor itself is powered independently from the UAV using a 10,000 mAh power bank (Adafruit, USA), enabling continuous operation for over 2 hours and allowing multiple sequential UAV flights without shutting down the sensor."

We also modified the text related to flight times in the newly added "Onboard Wind Measurements" section. The relevant text is here:

L. 242-243: "With the entire payload, including the methane sensor and anemometer components, the DJI Matrice 300 RTK UAV can achieve flight times of approximately 20 minutes."

The conclusion text was modified to read:

L. 592-594: "When the sensor is installed together with the anemometer assembly on a DJI Matrice 300 RTK UAV, several consecutive flights of approximately 20 minutes each can be carried out without needing to power off the sensor."

> What is the maximum altitude this system can reach?

The following text has been added:

L. 235-237: "We have deployed the sensor and UAV system at altitudes from approximately 0.5 to 40 m above takeoff, and we expect that higher flight altitudes would be achievable. In Canada, the maximum legal flight altitude is 122 m above ground level, for most UAV operations (Canadian Aviation Regulations, SOR96/433, s901.25, Government of Canada (2026))."

> Line 170: For both, vertical upward and downward operation? Are eddy-induced changes in wind velocity considered for downward flights?

We have focused on characterizing the 2D wind speed during horizontal flight only, because the flux curtains are comprised primarily of stacked horizontal transects. During flux quantification, we calculate the integrated methane flux density along each horizontal transect, neglecting the brief vertical flight segments. To clarify the onboard wind measurement methodology, we have added a new subsection to Methods titled "2.6 Onboard wind measurements," which describes the procedure for extracting the true wind speed and direction from onboard anemometer measurements. We have also added a new subsection to Results titled "3.3.1 Onboard wind measurements." This subsection contains the new Fig. 9 (see below) showing the raw and corrected wind measurements for the near curtain in the controlled-release. The corrected results are also compared with measurements from the stationary anemometer at the release point.

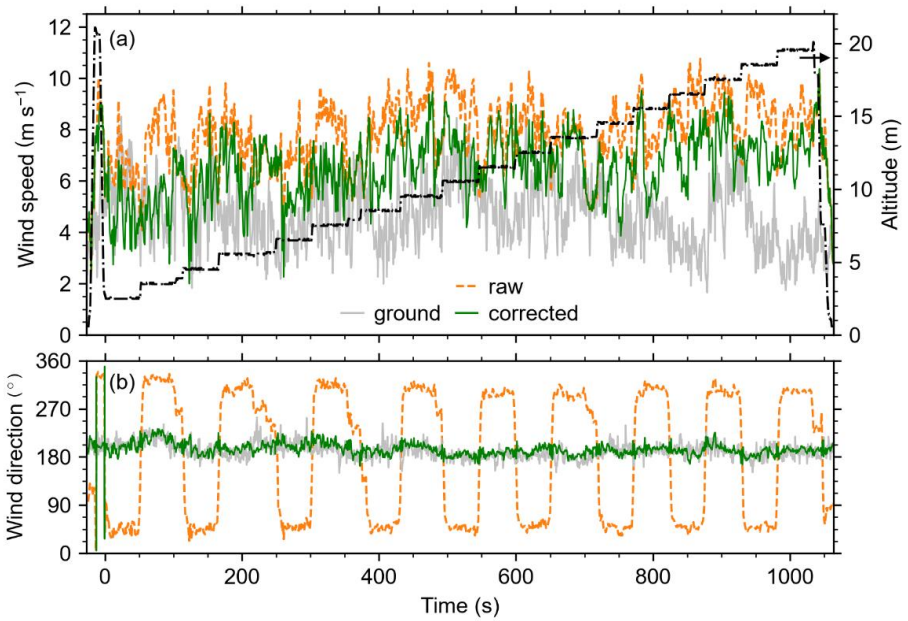

Figure 9. *Raw and corrected measurements of (a) wind speed (b) direction recorded by the onboard anemometer for the near curtain. Measurements from the stationary ground anemometer are shown for comparison. UAV height above takeoff is also shown in (a).*

Line 183: change “cames” to “comes”

This typo has been corrected.

Section 2.7:

Line 187: “flux curtain” pattern usually perform upwind flights as well, so that the background can be defined, without any disturbance from the point source. It is not clearly stated how the background value was defined for the two field missions.

We thank the reviewer for their question. The background was defined using downwind data collected from outside of the plume, similar to (Dooley et al., 2024; Morales et al., 2022). We use a peak-finding algorithm to identify and mask peaks within the timeseries data. Then we apply a moving average to the raw background data, using the optimal 5.8 s averaging window. Linear interpolation is used to estimate the background across the peaks. We also flew several upwind transects to confirm that no unidentified point sources were captured in the data. The background subtraction procedure is explained in detail in the new subsection “3.3.2 Background subtraction.”

L. 477-492: “For UAV-based measurements conducted within a few hundred meters of a known point source, the point source does not contribute to the slowly varying background (Morales et al., 2022; Dooley et al., 2024; Shah et al., 2020). Therefore, background methane mole fractions can be found either by flying transects upwind of the known source (Gordon et al., 2015) or using downwind data collected from outside of the plume (Morales et al., 2022). In some cases, where sensor drift or change is known to occur over the course of a measurement, averaging or fitting may be required to accurately define the baseline (Dooley et al., 2024). In this work, we use an averaging approach to extract the baseline from downwind transects. The approach is illustrated in Fig. 10. First, a peak-finding algorithm is used to identify peaks in the recorded methane timeseries data. A mask is defined around each peak such that the signal returns to the baseline on either side. By masking the peaks, we extract the raw background data. A 5.8 s moving average is applied to the background, where the 5.8 s window is chosen because it offers nearly optimal in-flight measurement precision, as determined from the Allan-Werle deviation (see Fig. 4). Linear interpolation is used to estimate the background across each of the peaks, where raw background data is not available. Finally, the elevated methane signal $[CH4]_{elev}$ is calculated by subtracting the averaged and interpolated background $[CH4]_{bkg}$ from the original measured methane data.

To confirm that no unidentified point sources were contributing to the observed methane enhancements, several transects were flown directly upwind of the release location. The timeseries data from the upwind flight showed no evidence of additional point sources.”

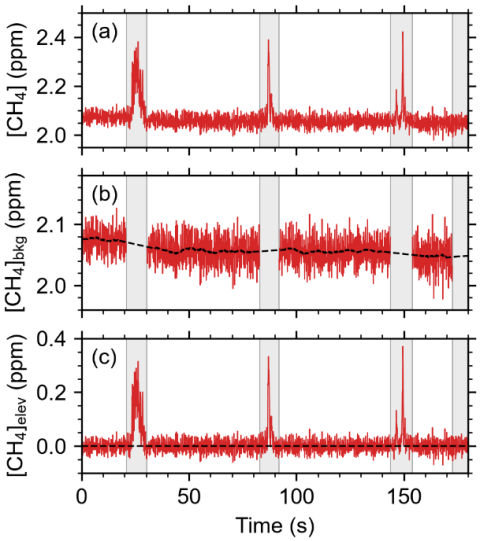

Figure 10. *Procedure for extracting the background methane mole fraction, illustrated for the far transect in controlled-release A. (a) Methane mole fraction timeseries at 10 Hz. Gray bars represent masks applied to each detected peak. (b) Background methane mole fraction with the peaks removed. The black dashed line is the 5.8 s moving average, with linear interpolation over the masked regions. (c) Elevated methane mole fraction.*

Section 3.1:

This section does quantify the sensors performance briefly, with three different approaches, but they all need to be more precise in discussing the sensors performance and limitations. According to the Allan-Werle deviation a minimum deviation of 3.4 ppb can be achieved at 5 s integration time, representing the optimal averaging time before instrumental drift becomes dominant. Of course, with faster time resolution, measurements can capture more atmospheric variability, but the atmospheric variability still needs to be larger than the instrumental variability. Furthermore, a total uncertainty estimation on the measured mixing ratios is missing (as mentioned in the general comments).

We thank the reviewer for their comments. As described above, we have significantly expanded the discussion of the sensor performance and uncertainty quantification. Changes include the addition of entirely new sections "3.2 Sensitivity to changing environmental conditions," "3.3.3 In-flight stability and performance," and "Appendix A: Uncertainty analysis for emission flux quantification." Section 3.3.3 reports the total uncertainty estimation for measured mixing ratios, with the relevant excerpt (L. 532-539) given on page 4 of this response letter.

Line 226: change "2 ppmv" to "ppm" and its mixing ratio not concentration!

"ppmv" has been changed to "ppm," and the terminology has been corrected to replace "concentration" with "mole fraction" throughout the manuscript.

Line 228: change "concentration" into mixing ratio and remove v/v.

This has been corrected.

Figure 2: Including the full H2O line would allow to track water vapor mixing ratios simultaneously, which may be useful for the water dilution effect correction for the wet methane mixing ratios. Although, depending on the phase of water during measurements, as droplets may cause issues.

We thank the reviewer for their comment. We were limited by the tuning range of the laser and it was not possible to record both the CH_4 line and the entire H_2O line with this laser diode. However, a detailed discussion of the effect of water vapour on the recorded CH_4 mole fraction has been added in the new section "3.2 Sensitivity to changing environmental conditions." The sensor's response to changing relative humidity is summarized in the new Fig. 7 (below).

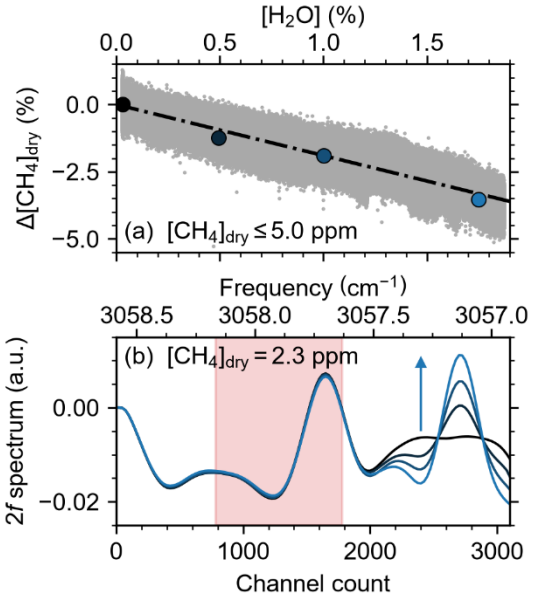

Figure 7. *(a) Relative change in the measured methane dry mole fraction as a function of water vapor mole fraction (approximately 0% to 80% R.H.), for methane dry mole fractions below 5 ppm. The dashed black line is a fit to the measured data. (b) 2f spectra for 2.3 ppm methane with water vapor mole fractions 0.03%, 0.5%, 1%, and 1.75%, corresponding to the large data points in (a). The arrow indicates increasing water vapor content. The shaded region indicates the bounds used to determine the peak-to-peak amplitude for methane.*

Lines 232 – 253: The sensor calibration was performed with mixing ratios ranging from 2 – 50 ppm. It would be interesting how the fitting curve and the comparison with the commercial methane sensors look like for more data points close to atmospheric typical mixing ratios. Higher mixing ratios also mean a stronger signal. How sensitive is the sensor to measure differences which are more likely to occur in the atmosphere? How are the uncertainties for mixing ratios close to 2 ppm, for both sensors?

We thank the reviewer for this suggestion. The sensor response is nearly linear with CH_4 mole fraction in the range of ~2-10 ppm. This can be seen in the revised Fig. 3, which depicts a calibration that was benchmarked against a newly acquired LICOR LI-7810 gas analyzer, providing a much more reliable reference. The calibration includes additional measurement points at mole fractions <5 ppm, and an inset that shows the calibration curve to be nearly linear in this range.

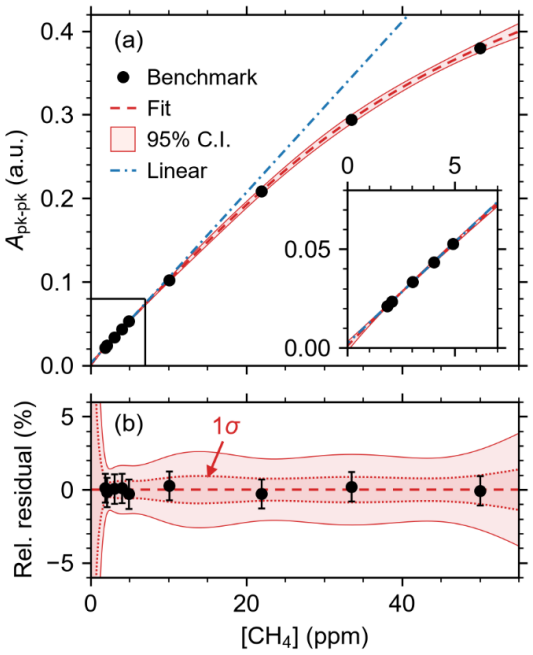

Figure 3. *(a) WMS 2f peak-to-peak amplitude as a function of methane mole fraction measured by benchmark instrument (LI-7810). Fit to Eq. 7 is shown with 95% confidence interval. For reference, a linear fit to the data points below 10 ppm is also shown. Inset shows expanded view of data points up to 5 ppm. (b) Relative residuals* $([CH4] - [CH4]_{fit})/[CH4]_{fit}$*, where error bars indicate 1% uncertainties on the methane mole fraction. The 1σ standard error on the fit is also shown.*

We also evaluated the ultra-lightweight (ULW) sensor response for rapidly varying CH_4 mole fractions in the range of ~2.2-3.2 ppm and compared the result to the commercial Aeris MIRA Pico and LICOR 7810 sensors (Fig. R4). The ULW sensor was placed in the calibration enclosure adjacent to a gas inlet shared by the Aeris MIRA Pico and the LICOR 7810. Building compressed air with a slightly elevated methane mole fraction flowed through the enclosure at a rate of 15 L min^{-1}. Small amounts of 8004 ppm CH_4 in synthetic air were injected, generating abrupt changes in the methane mole fraction. The ULW sensor and the Aeris MIRA Pico were both calibrated against the LICOR 7810 in the range of ~2-6 ppm. The data shown for the ULW sensor

corresponds to its intrinsic 100 Hz data rate. There was good agreement between the results reported by all three sensors over the 25-minute measurement period. Fig. R4(b) shows a more detailed view of the step at around 630 s, illustration the difference in response time between the three instruments. The sharp spike recorded by the ULW sensor at each step is correlated with the injection of 8004 ppm methane, before it fully mixes with the gas in the enclosure.

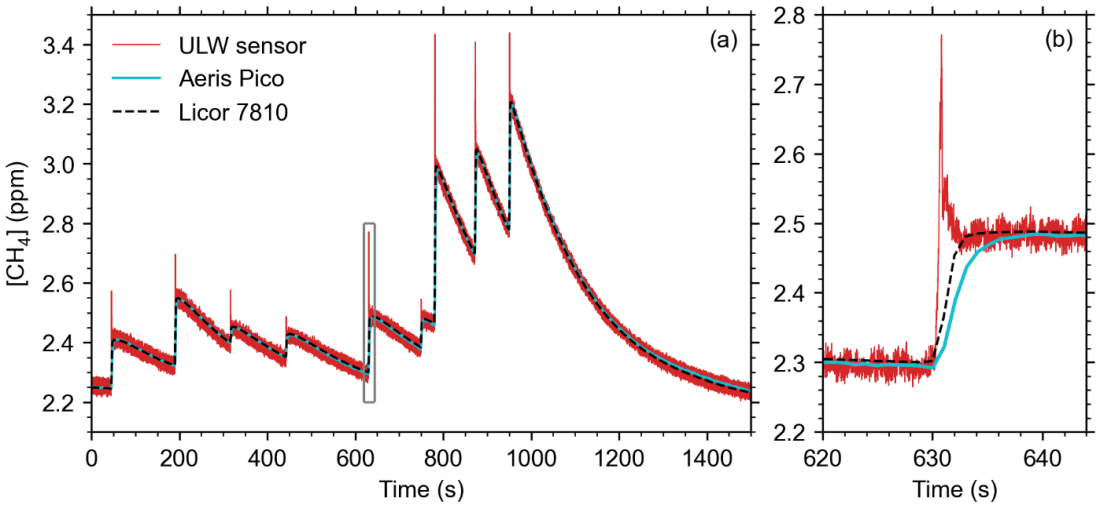

Figure R4. *(a) CH_4 mole fraction timeseries over 25-minute measurement period for the ULW sensor and commercial Aeris MIRA Pico and Licor 7810 sensors. (b) Expanded view of the region indicated by the gray box in (a).*

This controlled in-laboratory comparison demonstrates that the ULW sensor offers rapid response time and can accurately record changes in methane for mole fractions <3 ppm. However, the experiment does not demonstrate the impact of sensor drift experienced in field measurements, which may be significant for ambient CH_4 mole fraction measurement applications. In this work, we recorded slow in-flight drifts of around 50 ppb. This is shown in the new Fig. 11 and discussed in the new section "3.3.3 In-flight stability and performance." A comparison to the commercial Aeris MIRA Pico and Strato sensors is also now referenced in the text:

L. 488-490: "Drift is known to affect other UAV-borne sensors including commercial instruments such as the Aeris MIRA Pico and Strato sensors (Dooley et al., 2024; Bolek et al. 2026). Notably, Dooley et al. (2024) showed a systematic drift of roughly 250 ppb over a 20-minute UAV flight for a MIRA Pico sensor."

The average value of the background methane mole fraction recorded by the ULW sensor in controlled-release experiment A was 2.08±0.10 ppm. The estimated uncertainty includes statistical calibration error (3%), systematic error due to environmental conditions that differ from calibration conditions (5%), and measurement precision for an averaging time of 5.8 s (3.4 ppb).

> Lines 269-271: What about other error contributions? What about drift, sinusoidal structures? Please expand on the error contribution discussion here. Literature from Werle et al., 1993, 2011 or Röder et al., 2024 may help here.

In the revised manuscript, $\sqrt{1/\tau}$ lines have been included in the revised Fig. 4 as a reference for white noise. We have also revised the text to discuss deviations from white noise in greater detail. The relevant excerpt (L. 345-362) is given on pages 3-4 of this response letter.

> Figure 4: Is the timeseries a, b measured in 100Hz or 10Hz?

This is the intrinsic 100 Hz timeseries reported by the sensor. The figure caption has been updated to specify "100 Hz timeseries."

> Section 3.2:
>
> This section would benefit from a more real-world field experiment, maybe with a comparison to other methane sensors to show the instruments in-field performance.

We thank the reviewer for this suggestion. We strongly agree about the value of real-world field experiments and sensor intercomparisons. We have a second manuscript that has just been accepted for which we measured emissions from a naturally occurring geologic methane seep, including a comparison, in the context of emission quantification, to the commercially available Aeris MIRA Strato sensor deployed on a second UAV system (Bolek et al., 2026).

> Lines 278-279: This sentence sounds confusing.

The sentence was unnecessary and has been removed.

Lines 289: How do you measure the background?

A new subsection titled "3.3.2 Background subtraction" has been added. This section describes the process used to isolate methane enhancements from the background. See page 15-16 of this response letter.

Line 301: 2.1 ppm background level is quite high (see Lan et al., 2026). Are you sure that you have measured the background? Highest values at 8.2 ppm are also quite high. Is this realistic for "real" anthropogenic methane emission sources? Is there literature reporting similar values in the atmosphere from such anthropogenic sources?

We thank the reviewer for their observations. As described in the new section "3.3.2 Background subtraction," due to the near-field measurement condition, the controlled methane release does not contribute to the slowly varying background. Furthermore, transects flown directly upwind of the release point confirm that there were no other nearby point sources contributing to the enhancements observed in the measurement curtains. All measured enhancements above the baseline are therefore attributed to the controlled release. In the experiment labelled controlled-release B, the measurement site was located in close proximity to the Mer Bleue Bog in Ottawa, ON, Canada. This area is known to emit methane over a large area, resulting in elevated background levels (Moore et al., 2011).

Regarding the observed methane enhancements up to 8.2 ppm, similar or larger methane enhancements have been reported in the literature for UAV surveys of sources such as coal mining shafts (Andersen et al. 2021), landfills (Yong et al., 2024), natural gas compressor stations (Nathan et al., 2015), hydraulic fracturing facilities (Shah et al., 2020), and naturally occurring hydrocarbon gas seeps (Bolek et al., 2026) as well as controlled release studies designed to simulate emissions from anthropogenic sources (Bonne et al., 2024; Scheutz et al., 2025; Morales et al., 2022).

Lines 308-309: Why not? Either show the results and discuss them with literature why the controlled-release B did not work or not include this field mission B at all. It may be anyhow better to include here a direct comparison with another instrument in field close to, e.g., a real gas/oil leak to also show a possible application of this sensor and its advantages against other methane sensors.

We thank the reviewer for their question and their suggestion. Controlled-release B was not suitable for flux quantification due to the low wind speed and highly variable wind direction during the measurements. The mass-balance method relies on the assumption that wind fields are relatively stable throughout the curtain flight (Morales et al., 2022; Shaw et al., 2021). Some variability can be accounted for within the uncertainty analysis, but wind speeds <2.3 m s^{-1} and variability >33° (both observed during controlled-release B) have been associated with much higher residuals in controlled-release experiments (Morales et al., 2022). Controlled-release B was included in the original manuscript to acknowledge the limitations of the method.

Per the reviewer's suggestion, we have removed controlled-release B from the revised manuscript. In its place, we have included more detailed analysis of the sensor's in-flight performance and its response to changing environmental conditions. Comparison with another instrument in the field is the subject of a different manuscript (Bolek et al., 2026).

Section 3.3:

Line 314: Write always "Figure" instead of "Fig." if it starts the sentence.

This has been corrected.

Line 318: Is it defined somewhere how the calibration uncertainty is calculated?

As described above, the calibration uncertainty used for analyzing in-flight data is now discussed in more detail in Section 3.1 and the new section "3.3.3 In-flight stability and performance."

Line 319: The 26 ppb from the Allan-Werle plot represents the precision at integration times of 0.1s (see Werle et al., 1993).

The term "resolution" has been replaced with "precision" here and where applicable throughout the rest of the manuscript.

Line 320: Why is the background averaged over 60s? Explain why you chose this. And what do you mean with "resolution of 10 ppb"? Don't you mean a "precision of 10 ppb"?

We thank the reviewer for their question. We have revised the background subtraction procedure, using a 5.8 s averaging window instead of a 60 s window. The reason for this is explained in the new section "3.3.2 Background subtraction":

L. 485-486: "A 5.8 s moving average is applied to the background, where the 5.8 s window is chosen because it offers nearly optimal in-flight measurement precision, as determined from the Allan-Werle deviation (see Fig. 4)."

Line 320: "Min" is not defined. Replace ms-1 with ms-1.

The sentence has been revised and corrected:

L. 473: "… defined as the larger of 2% or 0.1 m s^{-1},…"

Figure 6: Have you measured the vertical wind speed or is vertical advection only derived from the model?

We do not measure the vertical wind speed. Most UAV-based mass-balance flux quantification approaches account only for horizontal wind, as the vertical wind is difficult to measure from a UAV and its contribution to the total flux is assumed to be negligible (Scheutz et al., 2025; Shaw et al., 2021). The logarithmic wind model is used to estimate the horizontal wind speed close to the ground.

Line 328: Not a complete sentence. Please repeat here briefly what the parameters mean for a better reading flow.

The revised text reads:

L. 554-557: "Fitting the logarithmic wind model (Eq. 6) to the wind data recorded from the UAV, friction velocity and surface roughness parameters $u^* = 0.842 \pm 0.024$ m s^{-1} and $z_0 = 0.340 \pm 0.029$ m, respectively, were obtained for the far flux curtain. For the near curtain, the parameters were found to be $u^* = 0.475 \pm 0.014$ m s^{-1} and $z_0 = 0.042 \pm 0.005$ m."

Line 330: What is the reason for the delay of 23 minute (e.g., logistics, battery charging)? Were calibrations performed in between?

This delay was related to flight planning logistics, including a technical problem uploading the flight plan to the UAV controller. We have clarified in the text that this was a "23-minute logistical delay."

Lines 332-333: Why is the far flux higher than the near flux? It falls within the uncertainty but could there be another explanation (e.g., wind, full plume advection into flight tracks only at far curtain, stronger uncertainties)? Particularly, as the mixing ratios were much higher in the near flux curtain.

We thank the reviewer for their question. The flux estimates for the near and far curtains are close to each other and well within the measurement uncertainty. The mixing ratios were higher in the near curtain because the gas is less dispersed when close to the emission source, as expected. Despite the difference in mixing ratios, due to the steady flow rate from the release point, the near-field measurement condition, the steady horizontal wind, and the scale of the measurement curtains, we expect the same total methane flux to pass through each of the curtains. The observed discrepancy is attributed to overall measurement and method uncertainties – particularly the interpolation and extrapolation components in the mass balance approach.

Line 338: Would be always beneficial to measure the whole vertical profile, but the plume propagation depends also a lot on local advection. Are there radiosonde profiles near by in upwind direction to somehow support this large flux underestimation without the extrapolation with the meteorological conditions?

We thank the reviewer for their comment. Unfortunately, there are no nearby radiosonde profiles available. It has been shown in the literature that, when applying the mass balance method to in-situ UAV-based measurements, missing transects through the centre of the plume can be a significant source of error (Mohammadloo et al., 2025; Andersen et al., 2021). In this work, the emission source was positioned only a few meters above the ground, and there was little opportunity for the plume to rise between the source and the measurement location. For both curtains, the highest mole fractions were observed in the lowest transect. By neglecting the lowest transect, which passes close to the plume center, we introduce a large discrepancy between the estimate and the true release rate. This is consistent with the findings by Moohammadloo (2025) and Andersen (2021), emphasizing the importance of sampling as close to the centre of the plume as possible.

Conclusion:

The conclusion should be considered to be structured differently. What is the key point of this paper? Start with the general construction of the instrument, then report laboratory and field performance, followed by the field evaluation of the sensor with the example missions. Clearly state what are the advantages of this sensor, and what are possible applications this sensor can be used for. Also discuss briefly its limitations and possible modifications, which may improve sensor performance or the variety of operation.

We thank the reviewer for their suggestions regarding the structure of the conclusion. The revised conclusion, which incorporates their feedback, is below:

L. 575-620: "In this work, we developed an ultra-lightweight and compact methane sensor platform for in-situ measurements and deployed it on a small enterprise-grade UAV in controlled-release experiments to evaluate its potential to quantify fugitive methane emissions. The sensor is based on tunable diode laser absorption spectroscopy and targets methane gas in the mid-IR using a HgCdTe photodetector and a GaSb-based DFB laser centered at 3270.4 nm. The instrument employs an open-path multi-pass absorption cell for fast response times (up to 100 Hz) and wavelength modulation spectroscopy for improved signal-to-noise. A small single board computer and custom data acquisition PCB has facilitated the miniaturization of a complete data acquisition and control system with real-time onboard WMS data processing and local data storage capabilities. Compared with its predecessor, the new instrument is 84% smaller, 75% lighter, and consumes 40% less power. Where possible, commercially available off-the-shelf components were used in the sensor design to facilitate the adoption and widespread use of this measurement technique. A lower-cost system could be achieved using silver or aluminum mirrors in place of gold and replacing the mid-IR light source and photodetector with near-IR alternatives for applications where the enhanced resolution provided by mid-IR sources is not required. Although our research demonstrates the sensor's application for methane, the same platform could be adapted to other gaseous species by substituting the laser and photodetector to target absorption features specific to the molecule of interest. Differences in atmospheric abundance or absorption cross section may require further optomechanical or electronics adaptations; however, the core design principles remain broadly transferable.

Weighing just 1.2 kg, including the dedicated battery, this is one of the lightest spectroscopic methane gas sensors reported to date. It is also extremely power efficient, consuming approximately 11 W of electrical power when the ambient temperature is around 20◦C, enabling continuous operation for more than 2 hours. When the sensor is installed together with the anemometer assembly on a DJI Matrice 300 RTK UAV, several consecutive flights of approximately 20 minutes each can be carried out sequentially without needing to power off the sensor.

The sensor achieves an in-flight precision of 6.6 ppb at 1 Hz which, to our knowledge, is the best 1 Hz precision for a UAV-borne methane sensor weighing less than 2 kg reported to date. The in-flight precision could be further improved by mitigating inductive noise produced by the sensor's on-board radio, used for real-time data streaming. Laboratory measurements without real-time data streaming show a 1 Hz precision of 3.7 ppb. When deployed on a fast-moving UAV platform traveling at 5-8 m s^{-1}, a 10 Hz time resolution is used for signal averaging, corresponding to an in-flight measurement precision of 26.5 ppb. In-flight drifts of up to 100 ppb were observed in the background methane signal over the course of a 20-minute flight, with the largest drifts seen at takeoff and landing. Drifts are attributed primarily to changes in ambient conditions and airflow. Laboratory experiments revealed a non-linear dependence on ambient air temperature and a linear dependence on water vapor mole fraction. Detailed characterization of these effects and improved on-board temperature and relative humidity measurements could facilitate the implementation of robust on-line corrections, which would enable more accurate quantification of background methane levels. However, sensor drift is not expected to be a dominant source of error when quantifying emissions from a near-by point source.

The system was deployed in a controlled-release experiment with a methane release rate of 0.48 kg h^{-1}, below the detection limit for most conventional aircraft methane sensing systems. Using a direct mass balance flux quantification approach, the true emission rate was obtained to within 9% under steady winds and at downwind distances of < 120 m from the release point. In this demonstration for which the methane source was positioned just a few meters above the ground, the accuracy of the retrieved emission rate was found to depend heavily on the lowest measured transects, which contained the highest methane content. To fully evaluate this UAV-based emission rate quantification approach, further systematic and statistical studies are needed to assess how variables such as meteorological conditions, source parameters, flight patterns, and terrain topography influence the probability of detection and quantification accuracy.

Overall, we have developed a high-precision ultra-lightweight gas sensor optimized for deployment on small UAVs. We have demonstrated that this is a promising method for targeted detection and quantification of emission sources near the ground and over terrain that is inaccessible to or cannot be measured by alternative measurement platforms. The platform is well suited for characterizing anthropogenic emissions from sources such as oil and gas facilities (well sites, compressor stations, gas processing plants), wastewater treatment facilities, and small landfills, and has also been used to quantify emissions from naturally occurring geologic gas seeps (Bolek et al., 2026). We have demonstrated promising detection and quantification capability at for emission rates near 0.5 kg h^{-1} and expect that even smaller sources could be characterized using this instrument by mitigating inductive noise or adapting flight strategies to accommodate longer averaging times, which would enhance the measurement precision. These results highlight the ultra-lightweight methane sensor's potential as a flexible and scalable solution for monitoring of methane emissions across a wide range of environments."

Line 345: Report here the maximum flight altitude, the drone and sensor can achieve.

The relevant text has been moved from the conclusion to the abstract and revised to read:

L. 1-2: "Uncrewed aerial vehicles (UAVs) offer versatile platforms for low-altitude (1 to 120 m) trace-gas measurements that can fill spatio-temporal measurement gaps between ground-based mobile platforms and conventional aircraft measurements."

Line 351: 100 Hz is not used for the atmospheric measurements. Change to 10 Hz.

We have revised the statement to read:

L. 579: "…for fast response times (up to 100 Hz)…"

The sensor's intrinsic data-rate is 100 Hz and signal averaging is applied in post-processing. Furthermore, two different averaging rates are applied in this paper: 0.1 s for the rapidly varying elevated signal and 5.8 s for the slowly varying background. Therefore, we feel that it is appropriate to report the intrinsic 100 Hz data-rate.

Line 353: "resolution" is used more for time or spatial resolution. Not for precisions! State other possible error uncertainties.

We have replaced "resolution" with "precision" and have added discussion related to sources of uncertainty that lead to drift, as described previously.

Line 357: Was 6.25% reported in the results part somewhere?

The values for the residual between the estimated and true emission rates have been added to the results section. The values are slightly different from those reported in the original manuscript because the controlled-release data has now been corrected to account for the effect of water vapor.

L. 562-563: "The true methane release rate, 0.48 kg h^{-1}, falls well within uncertainty for both estimated flux rates, differing by 8.7% for the far curtain and 1.1% for the near."

Lines 358-359: Yes, flux estimates closer to the ground had a ~50% contribution from this one field experiment, but this was derived from a model estimate. The drone did not fly that low. Please specify, and this statement is quite general for relying only on one example. Additional literature would help here.

We would like to clarify that we were referring in the discussion to impact of the lowest measured transect that was flown by the UAV, not to the extrapolated transects. However, we agree with the reviewer that the importance of the lowest measured transect is highly situation-dependent. Therefore, we have revised the statement to read:

L. 610-612: "In this demonstration for which the methane source was positioned just a few meters above the ground, the accuracy of the retrieved emission rate was found to depend heavily on the lowest measured transects, which contained the highest methane content."

Lines 360-362: Great! But add those points already in the discussions in the previous sections, so that you can conclude those here but not state them for the first time.

In addition to the expanded experimental sections that describe the sensor response to varying environmental conditions, we have added the following statements highlighting what further studies are needed:

L. 383-384: "Further study into the sensor's non-linear temperature-dependent response is needed facilitate the implementation of a robust correction protocol."

L. 404-405: "Experiments performed in a pressure-controlled environmental chamber are needed to thoroughly quantify how variations in pressure affect the sensor's response and to detect any response changes that are not related to spectral effects."

L. 530-531: "ore accurate and comprehensive onboard measurements of environmental conditions are needed to discern and mitigate the effects that impact the sensor's reading."

Literature:

Lan et al., 2026, https://doi.org/10.15138/P8XG-AA10

Curtius et al., 2024, https://doi.org/10.1038/s41586-024-08192-4

Karion et al., 2015, https://doi.org/10.1021/acs.est.5b00217

Conley et al., 2017, https://doi.org/10.5194/amt-10-3345-2017

Riese et al., 2025, https://doi.org/10.1175/BAMS-D-24-0232.1

Müller et al., 2015, https://doi.org/10.1002/2014GL062556

Ort et al., 2024, https://doi.org/10.5194/amt-17-3553-2024

D'Amato et al., 2025, https://doi.org/10.1364/OE.558437

Viciani et al., 2018, https://doi.org/10.3390/s18072380

Röder et al., 2024, https://doi.org/10.1007/s00340-024-08254-5

References

Andersen, T., Vinkovic, K., de Vries, M., Kers, B., Necki, J., Swolkien, J., Roiger, A., Peters, W., and Chen, H.: Quantifying methane emissions from coal mining ventilation shafts using an unmanned aerial vehicle (UAV)-based active AirCore system, Atmospheric Environment: X, 12, https://doi.org/10.1016/j.aeaoa.2021.100135, 2021.

Bolek, A., Heimann, M., and Göckede, M.: UAV-based in situ measurements of CO2 and CH4 fluxes over complex natural ecosystems, Atmospheric Measurement Techniques, 17, 5619–5636, https://doi.org/10.5194/amt-17-5619-2024, 2024.

Bolek, A., Beattie, M. N., Norooz Oliaee, J., MacLeod, R., Skeeter, J., Morse, P., Heimann, M., and Göckede, M.: Application of UAV-based methods for quantifying methane point source emissions over an Arctic geological seep, Atmospheric Measurement Techniques, 19, 3983–3998, https://doi.org/10.5194/amt-19-3983-2026, 2026.

Bonne, J. L., Donnat, L., Albora, G., Burgalat, J., Chauvin, N., Combaz, D., Cousin, J., Decarpenterie, T., Duclaux, O., Dumelié, N., Galas, N., Juery, C., Parent, F., Pineau, F., Maunoury, A., Ventre, O., Bénassy, M. F., and Joly, L.: A measurement system for CO2 and CH4 emissions quantification of industrial sites using a new in situ concentration sensor operated on board uncrewed aircraft vehicles, Atmospheric Measurement Techniques, 17, 4471–4491, https://doi.org/10.5194/amt-17-4471-2024, 2024.

Caulton, D. R., Li, Q., Bou-Zeid, E., Fitts, J. P., Golston, L. M., Pan, D., Lu, J., Lane, H. M., Buchholz, B., Guo, X., McSpiritt, J., Wendt, L., and Zondlo, M. A.: Quantifying uncertainties from mobile-laboratory-derived emissions of well pads using inverse Gaussian methods, Atmospheric Chemistry and Physics, 18, 15145–15168, https://doi.org/10.5194/acp-18-15145-2018, 2018.

Dang-Nhu, M., Pine, A. S., and Robiette, A. G.: Spectral Intensities in the v3 Bands of 12CH4, and 13CH4, Journal of Molecular Spectroscopy, 77, 57–68, 1979.

Donahue, C. P., Oberoi, K., Dillon, J. W., Hengst, V., Kennedy, B., Kearney, W., Lennox, J., Rehbein, E., Sykes, R., Dudiak, C. D., Altamura, D. T., Doherty, G., Roos, P. A., Brasseur, J. K., and Thorpe, M. J.: Aerial LiDAR-Based, Source-Resolved Methane Emissions Inventory: Permian Basin Case Study for Benchmarking U.S. Emissions, Environmental Science & Technology, 60, 13 968–13 979, https://doi.org/10.1021/acs.est.5c15184, 2026.

Dooley, J. F., Minschwaner, K., Dubey, M. K., Abbadi, S. H. E., Sherwin, E. D., Meyer, A. G., Follansbee, E., and Lee, J. E.: A new aerial approach for quantifying and attributing methane emissions: Implementation and validation, Atmospheric Measurement Techniques, 17, 5091–5111, https://doi.org/10.5194/amt-17-5091-2024, 2024.

Duren, R. M., Thorpe, A. K., Foster, K. T., Rafiq, T., Hopkins, F. M., Yadav, V., Bue, B. D., Thompson, D. R., Conley, S., Colombi, N. K., Frankenberg, C., McCubbin, I. B., Eastwood, M. L., Falk, M., Herner, J. D., Croes, B. E., Green, R. O., and Miller, C. E.: California's methane super-emitters, Nature, 575, 180–184, https://doi.org/10.1038/s41586-019-1720-3, 2019.

D'Amato, F., Barucci, M., Bianchini, G., and Viciani, S.: Quantum cascade laser (QCL) in airborne atmospheric measurements: A review [Invited], Optics Express, 33, 22 745, https://doi.org/10.1364/oe.558437, 2025.

El Abbadi, S. H., Chen, Z., Burdeau, P. M., Rutherford, J. S., Chen, Y., Zhang, Z., Sherwin, E. D., and Brandt, A. R.: Technological Maturity of Aircraft-Based Methane Sensing for Greenhouse Gas Mitigation, Environmental Science and Technology, 58, 9591–9600, https://doi.org/10.1021/acs.est.4c02439, 2024.

Gan, Q., Feng, Z., Zhang, D., Ma, S., Yang, X., and Yin, X.: High-Flow-Rate Trace Formaldehyde Detection Based on Ultraviolet Photoacoustic Spectroscopy Using a Long Resonant Photoacoustic Cell, Sensors, 26, https://doi.org/10.3390/s26051410, 2026.

Golston, L. M., Tao, L., Brosy, C., Schäfer, K., Wolf, B., McSpiritt, J., Buchholz, B., Caulton, D. R., Pan, D., Zondlo, M. A., Yoel, D., Kunstmann, H., and McGregor, M.: Lightweight mid-infrared methane sensor for unmanned aerial systems, Applied Physics B: Lasers and Optics, 123, https://doi.org/10.1007/s00340-017-6735-6, 2017.

Gordon, I., Rothman, L., Hargreaves, R., Gomez, F., Bertin, T., Hill, C., Kochanov, R., Tan, Y., Wcisło, P., Makhnev, V. Y., Bernath, P., Birk, M., Boudon, V., Campargue, A., Coustenis, A., Drouin, B., Gamache, R., Hodges, J., Jacquemart, D., Mlawer, E., Nikitin, A., Perevalov, V., Rotger, M., Robert, S., Tennyson, J., Toon, G., Tran, H., Tyuterev, V., Adkins, E., Barbe, A., Bailey, D., Bielska, K., Bizzocchi, L., Blake, T., Bowesman, C., Cacciani, P., ˇCermák, P., Császár, A., Denis, L., Egbert, S., Egorov, O., Ermilov, A. Y., Fleisher, A., Fleurbaey, H., Foltynowicz, A., Furtenbacher, T., Germann, M., Guest, E., Harrison, J., Hartmann, J.-M., Hjältén, A., Hu, S.-M., Huang, X., Johnson, T., Józwiak, H., Kassi, S., Khan, M., Kwabia-Tchana, F., Lee, T., Lisak, D., Liu, A.-W., Lyulin, O., Malarich, N., Manceron, L., Marinina, A., Massie, S., Mascio, J., Medvedev, E., Meshkov, V., Mellau, G. C., Melosso, M., Mikhailenko, S., Mondelain, D., Müller, H., O'Donnell, M., Owens, A., Perrin, A., Polyansky, O., Raston, P., Reed, Z., Rey, M., Richard, C., Rieker, G., Röske, C., Sharpe, S., Starikova, E., Stolarczyk, N., Stolyarov, A., Sung, K., Tamassia, F., Terragni, J., Ushakov, V., Vasilchenko, S., Vispoel, B., Vodopyanov, K., Wagner, G., Wójtewicz, S., Yurchenko, S., and Zobov, N.: The HITRAN2024 molecular spectroscopic database, Journal of Quantitative Spectroscopy and Radiative Transfer, p. 109807, https://doi.org/10.1016/j.jqsrt.2026.109807, 2026.

Gordon, M., Li, S. M., Staebler, R., Darlington, A., Hayden, K., O'Brien, J., and Wolde, M.: Determining air pollutant emission rates based on mass balance using airborne measurement data over the Alberta oil sands operations, Atmospheric Measurement Techniques, 8, 3745–3765, https://doi.org/10.5194/amt-8-3745-2015, 2015.

Government of Canada: Canadian Aviation Regulations, SOR/96-433, https://laws-lois.justice.gc.ca/eng/regulations/sor-96-433, 2026.

Herriott, D., Kogelnik, H., and Kompfner, R.: Off-Axis Paths in Spherical Mirror Interferometers, Applied Optics, 3, 523–526, 1964.

Kumar, P., Broquet, G., Yver-Kwok, C., Laurent, O., Gichuki, S., Caldow, C., Cropley, F., Lauvaux, T., Ramonet, M., Berthe, G., Martin, F., Duclaux, O., Juery, C., Bouchet, C., and Ciais, P.: Mobile atmospheric measurements and local-scale inverse estimation of the location and rates of brief CH4 and CO2 releases from point sources, Atmospheric Measurement Techniques, 14, 5987–6003, https://doi.org/10.5194/amt-14-5987-2021, 2021.

Maazallahi, H., Delre, A., Scheutz, C., Fredenslund, A. M., Schwietzke, S., Gon, H. D. V. D., and Röckmann, T.: Intercomparison of detection and quantification methods for methane emissions from the natural gas distribution network in Hamburg, Germany, Atmospheric Measurement Techniques, 16, 5051–5073, https://doi.org/10.5194/amt-16-5051-2023, 2023.

McDermitt, D., Burba, G., Xu, L., Anderson, T., Komissarov, A., Riensche, B., Schedlbauer, J., Starr, G., Zona, D., Oechel, W., Oberbauer, S., and Hastings, S.: A new low-power, open-path instrument for measuring methane flux by eddy covariance, in: Applied Physics B: Lasers and Optics, vol. 102, pp. 391–405, ISSN 09462171, https://doi.org/10.1007/s00340-010-4307-0, 2011.

Morales, R., Ravelid, J., Vinkovic, K., Korbe´n, P., Tuzson, B., Emmenegger, L., Chen, H., Schmidt, M., Humbel, S., and Brunner, D.: Controlled-release experiment to investigate uncertainties in UAV-based emission quantification for methane point sources, Atmospheric Measurement Techniques, 15, 2177–2198, https://doi.org/10.5194/amt-15-2177-2022, 2022.

Nathan, B. J., Golston, L. M., O'Brien, A. S., Ross, K., Harrison, W. A., Tao, L., Lary, D. J., Johnson, D. R., Covington, A. N., Clark, N. N., and Zondlo, M. A.: Near-Field Characterization of Methane Emission Variability from a Compressor Station Using a Model Aircraft, Environmental Science and Technology, 49, 7896–7903, https://doi.org/10.1021/acs.est.5b00705, 2015.

Norooz Oliaee, J., Sabourin, N. A., Festa-Bianchet, S. A., Gupta, J. A., Johnson, M. R., Thomson, K. A., Smallwood, G. J., and Lobo, P.: Development of a Sub-ppb Resolution Methane Sensor Using a GaSb-Based DFB Diode Laser near 3270 nm for Fugitive Emission Measurement, ACS Sensors, 7, 564–572, https://doi.org/10.1021/acssensors.1c02444, 2022.

Ort, L., Röder, L. L., Parchatka, U., Königstedt, R., Crowley, D., Kunz, F., Wittkowski, R., Lelieveld, J., and Fischer, H.: In-flight characterization of a compact airborne quantum cascade laser absorption spectrometer, Atmospheric Measurement Techniques, 17, 3553–3565, https://doi.org/10.5194/amt-17-3553-2024, 2024.

Röder, L. L., Ort, L., Lelieveld, J., and Fischer, H.: Quantitative analysis of temporal stability and instrument performance during field experiments of an airborne QCLAS via Allan–Werle-plots, Applied Physics B: Lasers and Optics, 130, https://doi.org/10.1007/s00340-024-08254-5, 2024.

Scheutz, C., Knudsen, J. E., Vechi, N. T., and Knudsen, J.: Validation and demonstration of a drone-based method for quantifying fugitive methane emissions, Journal of Environmental Management, 373, https://doi.org/10.1016/j.jenvman.2024.123467, 2025.

Shah, A., Pitt, J. R., Ricketts, H., Leen, J. B., Williams, P. I., Kabbabe, K., Gallagher, M. W., and Allen, G.: Testing the near-field Gaussian plume inversion flux quantification technique using unmanned aerial vehicle sampling, Atmospheric Measurement Techniques, 13, 1467–1484, https://doi.org/10.5194/amt-13-1467-2020, 2020.820

Shaw, J. T., Shah, A., Yong, H., and Allen, G.: Methods for quantifying methane emissions using unmanned aerial vehicles: A review, https://doi.org/10.1098/rsta.2020.0450, 2021.

Smith, B. J., Buckingham, S., Touzel, D. F., Corbett, A. M., and Tavner, C.: Development of Methods for Top-Down Methane Emission Measurements of Oil and Gas Facilities in an Offshore Environment Using a Miniature Methane Spectrometer and Long-Endurance Uncrewed Aerial System, in: SPE Production & Operations, vol. 565, pp. 565–577, Society of Petroleum Engineers, http://onepetro.org/PO/article-pdf/38/04/565/3309279/spe-206181-pa.pdf/1, 2023.

Takriti, M., Wynn, P. M., Elias, D. M., Ward, S. E., Oakley, S., and McNamara, N. P.: Mobile methane measurements: Effects of instrument specifications on data interpretation, reproducibility, and isotopic precision, Atmospheric Environment, 246, https://doi.org/10.1016/j.atmosenv.2020.118067, 2021.

Tettenborn, J., Zavala-Araiza, D., Stroeken, D., Maazallahi, H., Veen, C. V. D., Hensen, A., Velzeboer, I., Bulk, P. V. D., Vogel, F., Gillespie, L., Ars, S., France, J., Lowry, D., Fisher, R., and Röckmann, T.: Improving consistency in methane emission quantification from the natural gas distribution systems across measurement devices, Atmospheric Measurement Techniques, 18, 3569–3584, https://doi.org/10.5194/amt-18-3569-2025, 2025.

Tuzson, B., Graf, M., Ravelid, J., Scheidegger, P., Kupferschmid, A., Looser, H., Morales, R. P., and Emmenegger, L.: A compact QCL spectrometer for mobile, high-precision methane sensing aboard drones, Atmospheric Measurement Techniques, 13, 4715–4726, https://doi.org/10.5194/amt-13-4715-2020, 2020.

Werle, P.: Accuracy and precision of laser spectrometers for trace gas sensing in the presence of optical fringes and atmospheric turbulence, Applied Physics B: Lasers and Optics, 102, 313–329, https://doi.org/10.1007/s00340-010-4165-9, 2011.